

Spring 4-2015

Toward an Expanded Role for Collision-Induced Dissociation in Glycoproteomic Analysis

Venkata Kolli

University of Nebraska-Lincoln, venkata.kolli@huskers.unl.edu

Follow this and additional works at: <http://digitalcommons.unl.edu/chemistrydiss>



Part of the [Analytical Chemistry Commons](#)

Kolli, Venkata, "Toward an Expanded Role for Collision-Induced Dissociation in Glycoproteomic Analysis" (2015). *Student Research Projects, Dissertations, and Theses - Chemistry Department*. 55.
<http://digitalcommons.unl.edu/chemistrydiss/55>

This Article is brought to you for free and open access by the Chemistry, Department of at DigitalCommons@University of Nebraska - Lincoln. It has been accepted for inclusion in Student Research Projects, Dissertations, and Theses - Chemistry Department by an authorized administrator of DigitalCommons@University of Nebraska - Lincoln.

**Toward an Expanded Role for Collision-Induced Dissociation
in Glycoproteomic Analysis**

by

Venkata Karthik Kolli

A THESIS

**Presented to the Faculty of
The Graduate College at the University of Nebraska
In Partial Fulfillment of Requirements
For the Degree of Master of Science**

Major: Chemistry

Under the Supervision of Professor Eric D. Dodds

Lincoln, Nebraska

April 2015

Toward an Expanded Role for Collision-Induced Dissociation

in Glycoproteomic Analysis

Venkata Karthik Kolli, M.S.

University of Nebraska, 2015

Advisor: Eric D. Dodds

This thesis begins with an overview of the state-of-the-art in tandem mass spectrometry (MS/MS) analysis of glycopeptides. In this introduction, the primary focus is on utilization of different ion dissociation techniques for MS/MS to obtain structural information of N-glycopeptides. This includes a discussion of the importance of complementary MS/MS methods to attain complete structural characterization of N-glycopeptides. Emerging methods involving the use of a single ion dissociation technique for complete glycopeptide connectivity analysis were also presented. Next, the application of collision-induced dissociation (CID) to provide both amino acid sequence and monosaccharide connectivity for model N-glycopeptides was discussed in detail. Implementation of varying collision energies to generate energy-resolved breakdown curves suggested unique ranges of collision energies allowed glycan and peptide fragments to be obtained. An online collision energy modulation was demonstrated to allow both glycan and peptide fragments to be gathered in a single CID spectrum. Finally, the role of proton mobility in dictating the energy-resolved CID behaviors of N-glycopeptides was examined. Energy-resolved CID studies in the context of different precursor ion proton mobilities suggested the possibility that peptide and glycan cleavage products could be deliberately accessed at predictable collision energies.

Contents in Brief

Detailed Table of Contents	ii
Abbreviation and Symbols.....	iv
Index of Figures	vi
Index of Tables	viii
Acknowledgements.....	ix
Chapter 1 - Tandem Mass Spectrometry of Glycopeptides: A Brief Overview	1
Chapter 2 - Energy-Resolved Collision-Induced Dissociation Pathways of Model N-Linked Glycopeptides: Implications for Capturing Glycan Connectivity and Peptide Sequence in a Single Experiment	13
Chapter 3 - The Role of Proton Mobility in Determining the Energy-Resolved Vibrational Activation / Dissociation Channels of N-Glycopeptide Ions	48
Appendix A – Brief Summary of This Work.....	75

Detailed Table of Contents

Abbreviation and Symbols.....	iv
Index of Figures	vi
Index of Tables	viii
Acknowledgements.....	ix
Chapter 1 - Tandem Mass Spectrometry of Glycopeptides: A Brief Overview	1
Introduction.....	2
Overview of Glycan and Peptide Fragmentation.....	4
Application of MS/MS Methods to Glycopeptides	5
Overview.....	5
Use of Complementary MS/MS Methods.....	6
Use of a Single MS/MS Method.....	7
References.....	9
Chapter 2 - Energy-Resolved Collision-Induced Dissociation Pathways of Model N-Linked Glycopeptides: Implications for Capturing Glycan Connectivity and Peptide Sequence in a Single Experiment	13
Abstract.....	14
Introduction.....	15
Materials and Methods.....	19
Chemicals.....	19
Sample Preparation	19
Mass Spectrometry.....	20
Data Handling	21

Results and Discussion	21
CID of ECL Glycopeptide Ions	21
CID of BRB Glycopeptide Ions	28
Multi-Energy CID of the ECL and BRB Glycopeptides	34
Conclusions.....	37
References.....	42
Chapter 3 - The Role of Proton Mobility in Determining the Energy-Resolved	
Vibrational Activation / Dissociation Channels of N-Glycopeptide Ions	48
Abstract.....	49
Introduction.....	50
Materials and Methods.....	52
Reagents and Materials	52
Glycopeptide Preparation.....	52
Mass Spectrometry and Data Analysis	53
Results and Discussion	54
Overview.....	54
Precursor Ion Survival Curves	55
Energy-Resolved CID Comparisons at Various Proton Mobilities	59
CID Spectrum Comparisons at Various Proton Mobilities.....	66
Conclusions.....	69
References.....	71
Appendix A – Brief Summary of This Work.....	75

Abbreviations and Symbols

BRB	Bovine Ribonuclease B
CID	Collision-Induced Dissociation
CIR	Cleavage Intensity Ratio
ΔU	Static DC offset
e	Fundamental Charge
ECD	Electron Capture Dissociation
ECL	<i>Erythrina cristagalli</i> Lectin
E_k	Precursor Ion Kinetic Energy
$E_{k,n}$	Normalized Kinetic Energy
ETD	Electron Transfer Dissociation
eV	Electron Volts
f	Vibrational Degrees of Freedom
Fuc	Fucose
GlcNAc	N-acetylglucosamine
HCD	Higher-Energy Collisional Dissociation
HPLC	High Performance Liquid Chromatography
IRMPD	Infrared Multiphoton Dissociation
LC	Liquid Chromatography
m	Mass
Man	Mannose
MS	Mass Spectrometry
MS/MS	Tandem Mass Spectrometry

n_B	Number of Basic Amino Acid Residues
nESI	Nanoflow Electrospray Ionization
n_H	Number of Charge-Carrying Protons
PTM	Post-Translational Modification
Q-TOF	Quadrupole Time of Flight
SPE	Solid Phase Extraction
UVPD	Ultraviolet Photodissociation
V	Volts
Xyl	Xylose
z	Number of Charges
ZIC-HILIC	Zwitterionic Hydrophilic Interaction Liquid Interaction Chromatography

Index of Figures

Figure 1.1: Graphical summary of different approaches to glycoprotein analysis

Figure 1.2: Nomenclature for peptide and glycan fragments

Figure 2.1: CID of the triply protonated ECL glycopeptide with both glycan and peptide mass spectra

Figure 2.2: Energy resolved CID plot for the triply protonated ECL glycopeptide

Figure 2.3: CID of the doubly protonated ECL glycopeptide with both glycan and peptide mass spectra

Figure 2.4: Energy resolved CID plot for the doubly protonated ECL glycopeptide

Figure 2.5: CID of the doubly protonated BRB glycopeptide with both glycan and peptide mass spectra

Figure 2.6: Energy resolved CID plot for the doubly protonated BRB glycopeptide

Figure 2.7: CID of the triply protonated BRB glycopeptide with both glycan and peptide mass spectra

Figure 2.8: Energy resolved CID plot for the triply protonated BRB glycopeptide

Figure 2.9: Multi-energy CID of the triply protonated ECL glycopeptide

Figure 2.10: Multi-energy CID of the doubly protonated ECL glycopeptide

Figure 2.11: Multi-energy CID of the triply protonated BRB glycopeptide

Figure 2.12: Multi-energy CID of the doubly protonated BRB glycopeptide

Figure 3.1: Precursor ion survival curves for each of the glycopeptide ions studied

Figure 3.2: Energy-resolved breakdown curve for $[\text{NLTKDR} + \text{GlcNAc}_2\text{Man}_5 + 3\text{H}]^{3+}$ ($n_H > n_B$); $[\text{SRNLTK} + \text{GlcNAc}_2\text{Man}_5 + \text{H}]^{2+}$ ($n_H = n_B$); and $[\text{SRNLTKDR} + \text{GlcNAc}_2\text{Man}_5 + 2\text{H}]^{2+}$ ($n_H < n_B$) glycopeptide ions

Figure 3.3: Energy-resolved breakdown curve for $[\text{NLTK} + \text{GlcNAc}_2\text{Man}_5 + 2\text{H}]^{2+}$
glycopeptide ion

Figure 3.4: Energy-resolved breakdown curve for $[\text{SRNLTK} + \text{GlcNAc}_2\text{Man}_5 + 3\text{H}]^{3+}$
glycopeptide ion

Figure 3.5: Energy-resolved breakdown curve for $[\text{NLTK} + \text{GlcNAc}_2\text{Man}_5 + \text{H}]^+$
glycopeptide ion

Figure 3.6: Energy-resolved breakdown curve for $[\text{NLTKDR} + \text{GlcNAc}_2\text{Man}_5 + 2\text{H}]^{2+}$
glycopeptide ion

Figure 3.7: Energy-resolved breakdown curve for $[\text{SRNLTKDR} + \text{GlcNAc}_2\text{Man}_5 + 3\text{H}]^{3+}$ glycopeptide ion

Figure 3.8: CID spectra for the three $[\text{NLTKDR} + \text{GlcNAc}_2\text{Man}_5 + 3\text{H}]^{3+}$, $[\text{SRNLTK} + \text{GlcNAc}_2\text{Man}_5 + 2\text{H}]^{2+}$, and $[\text{SRNLTKDR} + \text{GlcNAc}_2\text{Man}_5 + 2\text{H}]^{2+}$ glycopeptide ions comprising majorly of glycan fragments

Figure 3.9: CID spectra for the three $[\text{NLTKDR} + \text{GlcNAc}_2\text{Man}_5 + 3\text{H}]^{3+}$, $[\text{SRNLTK} + \text{GlcNAc}_2\text{Man}_5 + 2\text{H}]^{2+}$, and $[\text{SRNLTKDR} + \text{GlcNAc}_2\text{Man}_5 + 2\text{H}]^{2+}$ glycopeptide ions comprising majorly of peptide fragments

Index of Tables

Table 2.1: CID collision energies corresponding to 50% precursor ion survival and the corresponding precursor ion charge state (z) and degrees of freedom (f)

Table 3.1: Potential differences and degrees of freedom normalized initial precursor ion kinetic energies resulting in 50% precursor ion survival of each glycopeptide studied

Table 3.2: Potential differences and degrees of freedom normalized initial precursor ion kinetic energies resulting in maximum proportion of glycosidic bond cleavage products and peptide backbone cleavage products to constitute 20% of integrated peak area for each glycopeptide ion

Acknowledgements

I would like to thank Dr. Eric Dodds for serving as my advisor. I would also thank him for his invariable support and guidance throughout this thesis work. Very special thanks for my thesis committee members Dr. David Hage, Dr. Robert Powers and Dr. Jian Zhang for their acceptance to serve in my thesis committee even at a short notice.

I would like to express my gratitude towards the Chemistry Department at University of Nebraska-Lincoln for their support and providing an opportunity to pursue my masters. I am grateful to Ron Cerny, Dr. Kurt Wulser and Carita Kordik for their technical assistance in the mass spectrometry instrumentation. I express my gratitude towards Dr. Ganga Fernando, Gabriela De La Cruz and Heidi Roth for their contributions in this project.

I express my gratitude for the support and friendship of Dodds group and other graduate students at UNL. I acknowledge my parents (Venkata Krishna Kolli & Sharada Kolli) and brother (Venkata Koushik Kolli) for their support throughout my masters program. I greatly thank my whole family and friends for their encouragement and guidance for pursuing my masters program.

Chapter 1

Tandem Mass Spectrometry of Glycopeptides: A Brief Overview

Portions of this chapter have appeared in:

V. Kolli, K. N. Schumacher, and E. D. Dodds, *Bioanalysis* 7: 113-131 (2015).

Introduction

Unlike the other building blocks of a cell, oligosaccharides are able to form branched structures of high complexity, and are thus considered among the most analytically challenging for structural characterization.¹ These challenges in structure determination become compounded when these oligosaccharides (or, glycans) occur in glycosylation, a post translational modification (PTM) of proteins.² Glycosylation plays significant roles in the functions of glycoproteins, and aberrant glycosylation can result from or lead to various diseases including cancer, neurodegenerative disorders, congenital disorders of glycosylation, and others.³⁻⁵ Understanding the compositional and structural features of glycoproteins in their full molecular complexity is essential to improving our understanding of their biological functions.

In general, glycosylation can be classified into the N- and O-linked types based on the site of glycan attachment to the polypeptide chain. If glycans are attached to the side chain of an asparagine residue in the context of an NXS or NXT sequon (with X being any amino acid other than proline), this is termed as N-linked glycosylation. On the other hand, if glycans are attached to the side chain of a serine or threonine residue, this is termed O-linked glycosylation.⁶ Several analytical methods have been implemented to characterize both N-linked and O-linked protein glycosylation. Among these methods, mass spectrometry (MS) stands out as a promising approach, partly due to recent advances in instrumentation to perform tandem mass spectrometry (MS/MS) analysis.⁷⁻¹⁰ These MS/MS methods can be implemented probe the structures of the glycoproteins by bringing about informative fragmentation processes. Due to their large structures and compositional heterogeneity, direct MS analysis of intact glycoproteins is seldom

performed. Currently, most work to characterize glycoproteins is done on simplified or isolated substructures of glycoproteins. Depending on the focus of interest, the MS based approaches for glycoprotein characterization can be broadly classified into three categories: glycomic approaches, proteomic approaches, or glycoproteomic approaches (**Figure 1.1**).¹¹ Among these three approaches, the work described in this thesis falls within the scope of glycoproteomic approaches, which consider both the glycan and peptide substructures, as well as their covalent connectivity. Such information is lost in the glycan-centered and protein-centered approaches. To thoroughly analyze intact glycopeptides, extensive research efforts have been directed towards development of MS/MS strategies which provide information on both the peptide and the glycan.

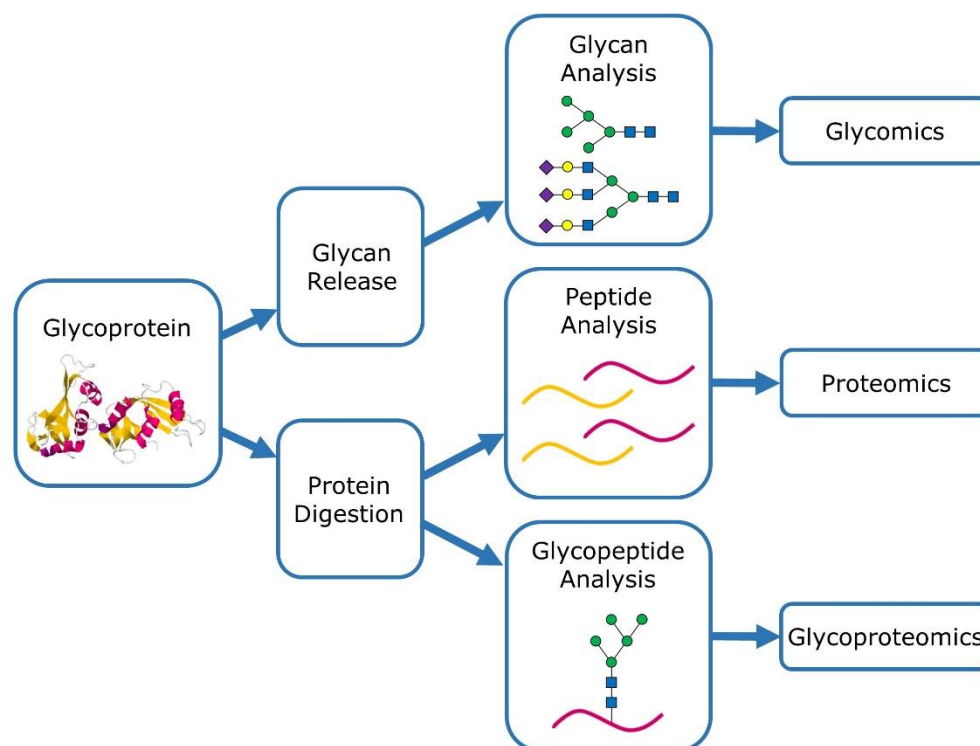


Figure 1.1. Graphical summary of different approaches to glycoprotein analysis. Broadly categorized, these include glycomics (characterization of glycans released from glycoproteins), proteomics (identification of glycoproteins based on analysis of their non-glycosylated proteolysis products), and glycoproteomics (characterization of site-specific connectivity between glycans and proteins through analysis of glycosylated proteolysis products). The work presented in this thesis is focused on glycoproteomics.

Overview of Glycan and Peptide Fragmentation

The basic scheme for MS/MS analysis involves mass selection of the target of interest. Subsequently, the precursor ions can be subjected to fragmentation using a variety of methods. Based on the location and type of cleavage, the resulting fragments can be labelled according to standard systems of nomenclature (**Figure 1.2**). In the case of glycans, the Domon and Costello nomenclature is followed for labelling the fragments.¹² According to this nomenclature, *B* and *Y* fragments are obtained when the glycosidic bond is cleaved, while *C* and *Z* fragments are obtained through cleavage of the adjacent bond on the other side of the glycosidic oxygen. Lastly, *A* and *X* fragments can be seen when cross-ring cleavages takes place. *A*, *B*, and *C* fragments retain the non-reducing end, while *X*, *Y*, and *Z* fragments retain the reducing end. Also, for *A* and *X*

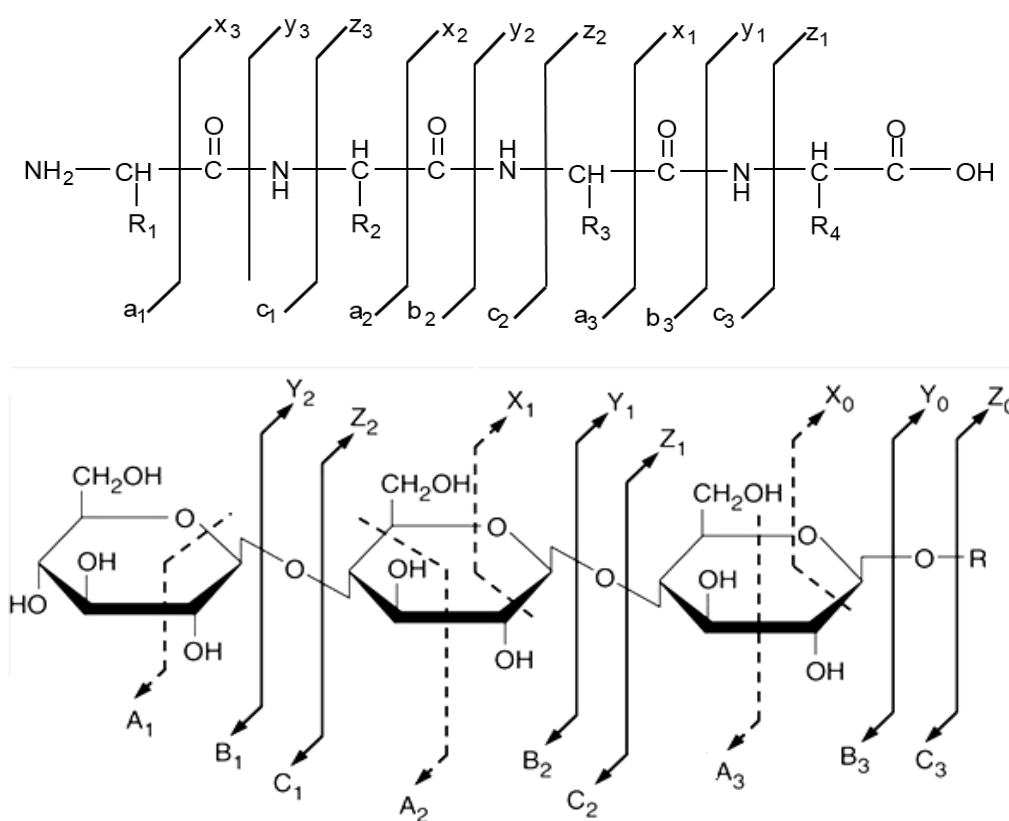


Figure 1.2. Nomenclature for peptide (top) and glycan (bottom) fragments.

fragments, the location of cross ring cleavages are shown as superscripts prior to the *A* or *X* letter.¹² Similarly for peptides, Roepstorff and Fohlman nomenclature is implemented.¹³ Here, *b* and *y* fragments represents the cleavage of the peptide amide bond, *c* and *z* fragments are from bond breakage between backbone N-C_α linkages, and lastly *a* and *x* fragments arise from cleavage of the bond linking the C_α- carbonyl carbon. Also, *a*, *b*, and *c* fragments will retain the N-terminus, while *x*, *y*, and *z* ions will contain the C-terminus.¹³ A brief overview of the various MS/MS techniques that result in these fragments follows.

Application of MS/MS Methods to Glycopeptides

Overview. The detection of putative glycopeptides by MS is usually followed by MS/MS in order to confirm the monosaccharide and amino acid composition, and to ascertain the monosaccharide connectivity and polypeptide sequence. While a glycopeptide MS/MS experiment would ideally reveal all of these features, the structural information actually obtained may or may not furnish this level of detail. Indeed, the information obtained in MS/MS experiments depends greatly upon the nature of the glycopeptide precursor ion (*e.g.*, composition, charge carrier, charge state, *etc.*) and the nature of the applied dissociation method (*e.g.*, vibrational activation, electron capture / electron transfer reactions, electronic excitation, *etc.*).¹¹ These considerations have been detailed in the context of glycopeptide analysis elsewhere.¹¹ The following will provide a brief discussion of recent developments and emerging strategies in the area of glycopeptide MS/MS analysis.

Use of complementary MS/MS methods. A variety of MS/MS methods are commonly applied to biomolecule analysis.¹⁴ Most prevalent among currently available techniques are those ion dissociation methods based upon either collisional vibrational activation, or electron capture / electron transfer reactions.¹⁵⁻¹⁷ Since these methods lead to structurally informative fragmentation processes through fundamentally different mechanisms, the outcomes of these MS/MS methods often yield complementary information. This complementarity has proven useful for proteomic analysis.¹⁸⁻¹⁹ Likewise, in the context of glycosylated peptide analysis, this orthogonality can be exploited in order to gain highly informative MS/MS data. It is now well known that, while vibrational activation / dissociation methods such as collision-induced dissociation (CID) and infrared multiphoton dissociation (IRMPD) most readily lead to preferential cleavage of glycosidic bonds, electron capture dissociation (ECD) and electron transfer dissociation (ETD) lead to selective scission of N-C α bonds along the polypeptide backbone.²⁰⁻²³ As a result, a number of glycopeptide analysis workflows have been devised in order to exploit multiple complementary MS/MS methods and thus gather more detailed structural information on glycopeptide ions. For instance, Alley *et al.* demonstrated a method based on LC-MS/MS with alternating CID and ETD events which was shown to allow extensive characterization of model glycopeptides.²⁴ In a similar fashion, Perdivara *et al.* and Darula *et al.* combined CID and ETD in order to characterize tryptic O-glycopeptides from biological mixtures.²⁵⁻²⁶ Analysis of N-glycopeptides was carried out by Cooper and coworkers using an LC-MS/MS method in which the observation of carbohydrate oxonium ions following CID was used to trigger ETD of the same precursor ion²⁷. In this way, CID and ETD were not simply alternated

during the entire LC-MS/MS run; rather, ETD was only carried out if the CID spectrum yielded evidence that a given precursor ion was a glycopeptide. CID neutral loss products can also be used to trigger ETD for only those analytes likely to be glycosylated.²⁸

Though not widely applied to glycopeptide analysis currently, we note that some previously reported hybrid MS/MS approaches have significant potential to extend the usefulness of MS/MS experiments that yield complementary structural information for glycopeptides.²⁹⁻³⁴

Use of a single MS/MS method. While the combination of two MS/MS methods can be highly informative regarding overall glycopeptide connectivity, significant effort has also been aimed at gaining extensive glycopeptide connectivity data using a single MS/MS technique. For example, photodissociation methods for MS/MS have achieved some success in this regard.³⁵⁻³⁶ Irradiation of trapped ions with infrared photons to bring about IRMPD is one such method³⁷. Studies by Adamson and Hakansson as well as Bindila *et al.* demonstrated the ability of IRMPD to yield significant information on both the glycan and peptide moieties of N-linked and O-linked glycopeptides, respectively.³⁸⁻³⁹ Lebrilla and coworkers also found IRMPD to effectively cleave both the carbohydrate and peptide groups of N- and O-glycopeptides, with their studies focused on the precursor ion characteristics (*e.g.*, composition, charge carrier, charge polarity) which tended to predispose a given precursor ion to one type of cleavage or the other.⁴⁰⁻⁴¹ Irradiation of precursor ions with ultraviolet photons to result in ultraviolet photodissociation (UVPD) has also found increased application to biomolecule MS/MS analysis in recent years.⁴²⁻⁴³ The work of Zhang and Reilly as well as Madsen and Brodbelt have established that UVPD yields concurrent fragmentation information on

both the glycan and the peptide for N-linked and O-linked glycopeptides, respectively.⁴⁴⁻

⁴⁵ In addition to photodissociation methods, certain CID-based strategies are being developed with the goal of gathering both the monosaccharide connectivity and amino acid sequence of glycopeptides. Such approaches are based on the observation that the applied collision energy dictates the dominant fragment ion types appearing in a CID spectrum. Thus, CID is capable of gaining broader use as a means of accessing peptide sequence ions in addition to the more frequently noted glycan fragmentation products. In the chapters that follow, work towards realizing these capabilities is presented.

References

1. Nilsson, J.; Halim, A.; Grahn, A.; Larson, G. *Glycoconjugate Journal* **2013**, *30*, 119-136.
2. Zaia, J. *Chemistry & Biology* **2008**, *15*, 881-92.
3. Galligan, J. J.; Fritz, K. S.; Tipney, H.; Smathers, R. L.; Roede, J. R.; Shearn, C. T.; Hunter, L. E.; Petersen, D. R. *Journal of Proteome Research* **2011**, *10*, 1837-47.
4. Song, E.; Pyreddy, S.; Mechref, Y. *Rapid Communications in Mass Spectrometry : RCM* **2012**, *26*, 1941-54.
5. Schiel, J. E. *Analytical and Bioanalytical Chemistry* **2012**, *404*, 1141-9.
6. Varki, A.; Etzler, M. E.; Cummings, R. D.; Esko, J. D. Discovery and Classification of Glycan-Binding Proteins. In *Essentials of Glycobiology*, 2nd ed.; Varki, A.; Cummings, R. D.; Esko, J. D.; Freeze, H. H.; Stanley, P.; Bertozzi, C. R.; Hart, G. W.; Etzler, M. E., Eds. Cold Spring Harbor (NY), 2009.
7. Patwa, T.; Li, C.; Simeone, D. M.; Lubman, D. M. *Mass Spectrometry Reviews* **2010**, *29*, 830-44.
8. Wuhrer, M. *Glycoconjugate Journal* **2013**, *30*, 11-22.
9. Wuhrer, M.; Catalina, M. I.; Deelder, A. M.; Hokke, C. H. *Journal of Chromatography. B* **2007**, *849*, 115-28.
10. Dodds, E. D. *Mass Spectrometry Reviews* **2012**, *31*, 666-82.
11. Kolli, V.; Schumacher, K. N.; Dodds, E. D. *Bioanalysis* **2015**, *7*, 113-131.
12. Domon, B.; Costello, C. E. *Glycoconjugate Journal* **1988**, *5*, 397-409.
13. Roepstorff, P.; Fohlman, J. *Biomedical Mass Spectrometry* **1984**, *11*, 601.

14. Sleno, L.; Volmer, D. A. *Journal of Mass Spectrometry* **2004**, *39*, 1091-1112.
15. Zubarev, R. A. *Mass Spectrometry Reviews* **2003**, *22*, 57-77.
16. Pitteri, S. J.; McLuckey, S. A. *Mass Spectrometry Reviews* **2005**, *24*, 931-958.
17. Mayer, P. M.; Poon, C. *Mass Spectrometry Reviews* **2009**, *28*, 608-639.
18. Coon, J. J. *Analytical Chemistry* **2009**, *81*, 3208-3215.
19. Zubarev, R. A.; Zubarev, A. R.; Savitski, M. M. *Journal of the American Society for Mass Spectrometry* **2008**, *19*, 753-761.
20. Hakansson, K.; Cooper, H. J.; Emmett, M. R.; Costello, C. E.; Marshall, A. G.; Nilsson, C. L. *Analytical Chemistry* **2001**, *73*, 4530-4536.
21. Hakansson, K.; Chalmers, M. J.; Quinn, J. P.; McFarland, M. A.; Hendrickson, C. L.; Marshall, A. G. *Analytical Chemistry* **2003**, *75*, 3256-3262.
22. Hogan, J. M.; Pitteri, S. J.; Chrisman, P. A.; McLuckey, S. A. *Journal of Proteome Research* **2005**, *4*, 628-632.
23. Han, H.; Xia, Y.; Yang, M.; McLuckey, S. A. *Analytical Chemistry* **2008**, *80*, 3492-3497.
24. Alley, W. R., Jr.; Mechref, Y.; Novotny, M. V. *Rapid Communications in Mass Spectrometry* **2009**, *23*, 161-170.
25. Perdivara, I.; Petrovich, R.; Allinquant, B.; Deterding, L. J.; Tomer, K. B.; Przybylski, M. *Journal of Proteome Research* **2009**, *8*, 631-642.
26. Darula, Z.; Chalkley, R. J.; Baker, P.; Burlingame, A. L.; Medzihradszky, K. F. *European Journal of Mass Spectrometry* **2010**, *16*, 421-428.
27. Singh, C.; Zampronio, C. G.; Creese, A. J.; Cooper, H. J. *Journal of Proteome Research* **2012**, *11*, 4517-4525.

28. Chen, R.; Wang, F.; Tan, Y.; Sun, Z.; Song, C.; Ye, M.; Wang, H.; Zou, H. *Journal of Proteomics* **2012**, *75*, 1666-1674.
29. Hashimoto, Y.; Hasegawa, H.; Yoshinari, K.; Waki, I. *Analytical Chemistry* **2003**, *75*, 420-425.
30. Tsybin, Y. O.; Witt, M.; Baykut, G.; Kjeldsen, F.; Hakansson, P. *Rapid Communications in Mass Spectrometry* **2003**, *17*, 1759-1768.
31. Zubarev, R. A.; Witt, M.; Baykut, G. *Analytical Chemistry* **2005**, *77*, 2992-2996.
32. Dodds, E. D.; Hagerman, P. J.; Lebrilla, C. B. *Analytical Chemistry* **2006**, *78*, 8506-8511.
33. Mihalca, R.; van der Burgt, Y. E.; McDonnell, L. A.; Duursma, M.; Cerjak, I.; Heck, A. J.; Heeren, R. M. *Rapid Communications in Mass Spectrometry* **2006**, *20*, 1838-1844.
34. Dodds, E. D.; German, J. B.; Lebrilla, C. B. *Analytical Chemistry* **2007**, *79*, 9547-9556.
35. Dunbar, R. C. *International Journal of Mass Spectrometry* **2000**, *200*, 571-689.
36. Brodbelt, J. S. *Journal of the American Society for Mass Spectrometry* **2011**, *22*, 197-206.
37. Brodbelt, J. S.; Wilson, J. J. *Mass Spectrometry Reviews* **2009**, *28*, 390-424.
38. Adamson, J. T.; Hakansson, K. *Journal of Proteome Research* **2006**, *5*, 493-501.
39. Bindila, L.; Steiner, K.; Schaffer, C.; Messner, P.; Mormann, M.; Peter-Katalinic, J. *Analytical Chemistry* **2007**, *79*, 3271-3279.
40. Seipert, R. R.; Dodds, E. D.; Clowers, B. H.; Beecroft, S. M.; German, J. B.; Lebrilla, C. B. *Analytical Chemistry* **2008**, *80*, 3684-3692.

41. Seipert, R. R.; Dodds, E. D.; Lebrilla, C. B. *Journal of Proteome Research* **2009**, *8*, 493-501.
42. Ly, T.; Julian, R. R. *Angewandte Chemie International ed* **2009**, *48*, 7130-7137.
43. Reilly, J. P. *Mass Spectrometry Reviews* **2009**, *28*, 425-447.
44. Zhang, L.; Reilly, J. P. *Journal of Proteome Research* **2009**, *8*, 734-742.
45. Madsen, J. A.; Ko, B. J.; Xu, H.; Iwashkiw, J. A.; Robotham, S. A.; Shaw, J. B.; Feldman, M. F.; Brodbelt, J. S. *Analytical Chemistry* **2013**, *85*, 9253-9261.

Chapter 2

Energy-Resolved Collision-Induced Dissociation Pathways of Model N-Linked Glycopeptides: Implications for Capturing Glycan Connectivity and Peptide Sequence in a Single Experiment

Portions of this chapter have appeared in:

V. Kolli and E. D. Dodds, *Analyst* 139: 2144-2153 (2014).

Abstract

Tandem mass spectrometry (MS/MS) of glycopeptides stands among the principal analytical approaches for assessing protein glycosylation in a site-specific manner. The aims of such experiments are often to determine the monosaccharide connectivity of the glycan, the amino acid sequence of the peptide, and the site of glycan attachment. This level of detail is often difficult to achieve using any single ion dissociation method; however, precedent does exist for use of collision-induced dissociation (CID) to establish either the connectivity of the oligosaccharide or the sequence of the polypeptide depending upon the applied collision energy. Unfortunately, the relative energy requirements for glycan and peptide cleavage have not been thoroughly characterized with respect to specific physicochemical characteristics of the precursor ions. This report describes case studies on the energy-resolved CID pathways of model tryptic glycopeptides derived from *Erythrina cristagalli* lectin and bovine ribonuclease B. While glycopeptide ions having disparate physical and chemical characteristics shared strikingly similar qualitative responses to increasing vibrational energy deposition, the absolute collision energies at which either glycan or peptide fragmentations were accessed varied substantially among the precursor ions examined. Nevertheless, these data suggest that the energy requirements for peptide and glycan cleavage may be somewhat predictable based on characteristics of the precursor ion. The practical usefulness of these observations was demonstrated through implementation of online collision energy modulation such that both glycan and peptide fragmentation were captured in the same spectrum, providing near-exhaustive glycopeptide characterization in a single

experiment. Overall, these results highlight the potential to further extend the capabilities of CID in the context of glycoproteomics.

Introduction

The site-specific analysis of protein glycosylation in complex biological samples stands among the grand challenges facing modern post-genomic science.¹⁻⁵ Accordingly, there exists a strong demand for glycoproteomic capabilities to facilitate determination of site-specific glycosylation in biological mixtures. This interest has been motivated in large part by a continually expanding appreciation of protein-modifying oligosaccharides as they pertain to numerous biological processes (*e.g.*, fertilization; immune recognition; host-pathogen interaction; *etc.*) and human disease states (*e.g.*, cancer; congenital disorders of glycosylation; neurodegenerative disorders, *etc.*).⁶⁻¹⁷ While protein glycosylation analyses are often carried out with either a “glycocentric” (*i.e.*, compositional and structural analysis of glycans released from glycoproteins) or a “proteocentric” (*i.e.*, identification of deglycosylated glycoproteins with indirect glycosylation site localization) outlook, the loss of molecular detail imposed by glycan release limits the specificity and potential for biological resolution that can be furnished by such analyses.¹⁸ In order to map specific oligosaccharide structures to their corresponding sites of protein attachment, the analytical scheme must preserve the oligosaccharide-polypeptide connectivity until such a time that the chosen approach can characterize the linkage.

One means of addressing this task entails the adaptation of bottom-up methods for mass spectrometry (MS) based proteomics to characterize glycopeptides.¹⁹⁻²¹ While

advantageous in terms of directness (glycan release is avoided, thus attachment sites need not be merely inferred), this approach is subject to a number of analytical challenges.^{22, 23} The acquisition and subsequent interpretation of informative tandem mass spectrometry (MS/MS) data for glycopeptide ions stand among the most pressing of these challenges. Significant effort has been made to maximize the information content of glycopeptide ion dissociation spectra, including those obtained through vibrational activation / dissociation methods such as collision-induced dissociation (CID)^{24, 25} and infrared multiphoton dissociation (IRMPD);^{26, 27} ion-electron and ion-ion reactions resulting in electron capture dissociation (ECD)^{28, 29} or electron transfer dissociation (ETD);^{30, 31} and irradiation with ultraviolet photons in order to achieve ultraviolet photodissociation (UVPD).^{32, 33} One useful outcome of these investigations has been the observation of a high degree of complementarity between the vibrational activation / dissociation spectra and the electron capture / transfer dissociation spectra of glycopeptide ions. A number of researchers have noted that while CID and IRMPD tend to preferentially cleave the oligosaccharide moiety, ECD and ETD characteristically result in cleavage of only the polypeptide backbone.³⁴⁻³⁸ This general behavior has proven very valuable, as application of two complementary methods can enable thorough characterization of glycopeptide composition and structure.³⁹⁻⁴³ Unsurprisingly, a number of other glycopeptide ion dissociation pathways have been observed which do not fall within the domain of strictly complementarity vibrational activation / dissociation and electron transfer / capture dissociation.⁴⁴⁻⁴⁷ This includes numerous examples of vibrational activation / dissociation methods providing information not limited to the carbohydrate group, but extending to the amino acid sequence of the peptide group as well. For example, fragmentation of

glycopeptide amino acid chains has been noted in IRMPD,^{26, 27, 48, 49} low-energy beam-type CID,⁵⁰⁻⁵⁴ and high-energy beam-type CID.⁵⁵⁻⁵⁷ As noted in these studies, the energy required to achieve scission of the peptide backbone is generally much greater than that necessary for cleavage of the glycan group. These energy-resolved fragmentation channels are of significant analytical utility; however, the various dissociation pathways have not been thoroughly studied with respect to specific physical and chemical characteristics of glycopeptide precursor ions. In particular, the present understanding of factors which dictate the energetic requirements for peptide backbone fragmentation is not well developed, despite even relatively recent energy-resolved CID studies of glycopeptides (which did not investigate the fragmentation of the peptide group).^{25, 58} This type of understanding would be of great practical use, as it could conceivably allow precursor ion characteristics to inform the setting of CID collision energies such that glycan or peptide cleavages are more deliberately accessed. If well characterized, the diverse fragmentation pathways of glycosylated peptide ions can be highly advantageous in increasing the density of structural information yielded by MS/MS. Moreover, as essentially all MS/MS instruments are capable of CID, the ability to extract maximum structural information regarding both the oligosaccharide and the polypeptide using low-energy vibrational activation / dissociation alone is particularly appealing.

The research reported here is focused upon a detailed study of the energy-resolved CID characteristics of tryptic glycopeptides chosen as models for this study due to their disparate characteristics. The first of these was a 17 amino acid glycopeptide carrying a seven monosaccharide paucimannosidic glycan (*i.e.*, containing the trimannosyl core with added fucose and xylose residues). The second was a six amino acid glycopeptide

carrying a seven monosaccharide high mannose glycan (*i.e.*, containing the trimannosyl core with added mannose residues). These model glycopeptides, each harboring two basic amino acid side chains, were studied as their doubly protonated and triply protonated precursor ions. This allowed the energy requirements of the various fragmentation pathways to be evaluated both in the presence and absence of readily mobile protons. Although there were considerable quantitative differences in the absolute collision energies at which different dissociation channels were accessed, these experiments revealed a striking concordance with respect to qualitative trends in the energy-resolved CID behaviors of these analytes. In all cases, *Y*-type fragmentations of the oligosaccharide group comprised the lowest-energy dissociation pathways; however, with increasing vibrational energy deposition these primary fragment ions gave rise to secondary product ions dominated by the Y_1 fragment (peptide plus reducing terminal monosaccharide) and ultimately a collection of tertiary fragments including the Y_0 fragment (complete glycan loss) and an abundance of peptide *b* and *y* fragments. Despite the quantitative differences in energy-resolved CID of the precursor ions examined, these data suggest that key dissociation characteristics may be somewhat predictable based on characteristics of the precursor ion. Finally, these observations enabled the design and implementation of a multi-energy CID experiment which permitted different energy-resolved dissociation channels to be captured in a single information-rich CID spectrum which yielded both the glycan connectivity and the amino acid sequence. In summary, the present results suggest means of taking more complete advantage of CID capabilities for glycopeptide structure characterization.

Materials and Methods

Chemicals. Bovine ribonuclease B (BRB), ammonium bicarbonate, urea, dithiothreitol, iodoacetamide, proteomics grade trypsin, imidazole, and formic acid were purchased from Sigma-Aldrich (St. Louis, MO, USA). *Erythrina cristagalli* lectin (ECL) was obtained from Vector Labs (Burlingame, CA, USA). HPLC grade acetonitrile was acquired from Fisher Scientific (Fair Lawn, NJ, USA). HPLC grade water was purchased from Burdick & Jackson (Muskegon, MI, USA).

Sample preparation. For each glycoprotein of interest, a 50 μL aliquot of 2 $\mu\text{g}/\mu\text{L}$ glycoprotein solution in 8 M urea and 50 mM NH_4HCO_3 (pH 7.5) was treated with 10 μL of 450 mM dithiothreitol in 50 mM NH_4HCO_3 (pH 7.5). This mixture was incubated for 1 h at 55°C for disulfide bond reduction. A 10 μL portion of 500 mM iodoacetamide in 50 mM NH_4HCO_3 (pH 7.5) was then added. This was followed by incubation for 1 h in the dark at ambient temperature for thiol acetamidation. The urea content of the sample was then diluted to < 2 M by addition of 175 μL 50 mM NH_4HCO_3 (pH 7.5). A 5 μL aliquot of 0.5 $\mu\text{g}/\mu\text{L}$ of trypsin was next added, and this solution was allowed to incubate for 18 hours at 37°C. The digest was subsequently vacuum centrifuged using a Speed Vac SC110 (Thermo Savant, Holbrook, NY, USA) to reduce the volume of the solution to approximately 10 μL . The digest was reconstituted to a total volume of 100 μL by addition of 0.1% formic acid. To enrich the glycosylated fraction of tryptic peptides, solid phase extraction was performed using zwitterionic hydrophilic interaction liquid chromatography (ZIC-HILIC) in a pipette tip format (Protea Biosciences, Somerset, NJ, USA). Each ZIC-HILIC tip was wetted with water, equilibrated with 80% acetonitrile / 0.1% formic acid, then loaded with a portion of the reconstituted digest in 80%

acetonitrile (*i.e.*, 4 μL of reconstituted digest plus 16 μL acetonitrile). Each tip was then washed with 80% acetonitrile / 0.1% formic acid. Finally, elution was performed using 0.1% formic acid.

Mass spectrometry. All analyses were conducted using a Synapt G2 HDMS quadrupole time of flight (Q-TOF) hybrid mass spectrometer (Waters, Manchester, UK). The instrument was fitted with a home-built static nanoflow electrospray ionization (nESI) stage which delivered the capillary potential by means of a platinum wire placed in contact with a small portion of analyte solution contained in a borosilicate emitter. Samples of approximately 10 μL purified digest or purified digest spiked to include 10 mM in imidazole (to enhance the abundance of lower charge states produced by nESI) were placed into nESI emitters using a 10 μL syringe (Hamilton, Reno, NV, USA). The emitters were fashioned in-house from 1.5 - 1.8 x 100 mm Corning Pyrex melting point capillaries (Corning, NY, USA) using a vertical micropipette pipette puller (David Kopf Instruments, Tujunga, CA, USA). Ionization by nESI was conducted using a capillary potential of 1.0 - 1.4 kV, a sampling cone voltage of 15 - 35 V, and an extraction cone voltage of 2 - 4 V. Source temperature was maintained at 80°C. Precursor ions of interest were quadrupole selected and subjected to CID such that the trap region stacked ring ion guide of the instrument served as the collision cell. Argon was used as the collision gas at a pressure of approximately 5.0×10^{-3} mbar within the collision cell. Collision energy was modulated by adjusting the static DC offset (ΔU) between the collision cell and the stacked ring ion guide of the ion source region. Direct infusion spectra were acquired for approximately one minute.

Data handling. Spectrum acquisition and analysis was performed in MassLynx 4.1 (Waters), and further data processing and visualization were carried out using SigmaPlot 10.1 (Systat, Chicago, IL, USA) and using custom routines written and implemented in IGOR Pro 6.3 (WaveMetrics, Lake Oswego, OR, USA). Where practical, product ions resulting from cleavage of the carbohydrate group were assigned according to the nomenclature of Domon and Costello.⁵⁹ Occasionally, glycan fragmentations or combinations thereof could not be unambiguously or conveniently assigned using these formalisms. In such instances, the fragments were assigned by indicating monosaccharide losses from the precursor. Product ions involving scission of the peptide were assigned in accord with the nomenclature of Roepstorff and Fohlman.⁶⁰ When naming and referring to product ions, lower case letters were used to specify peptide fragmentation, while upper case letters were used to indicate oligosaccharide cleavage. For the sake of clarity, product ions resulting from small neutral losses (*e.g.*, H₂O, NH₃) from the precursor or other fragments were assigned but not labelled in the spectra presented below. Glycan structures were diagrammed using the monosaccharide symbology of Varki *et al.*⁶¹ Peptide sequences were presented using standard one-letter amino acid notation, while monosaccharide names were abbreviated as follows: GlcNAc, N-acetylglucosamine; Man, mannose; Fuc, fucose; Xyl, xylose.

Results and Discussion

CID of ECL glycopeptide ions. Upon nESI-MS analysis, the ZIC-HILIC purified tryptic digests of ECL yielded a major peak corresponding to the glycopeptide ion [SKPAQGYGYLGVFNNNSK + GlcNAc₂ Man₃ Fuc₁ Xyl₁ + 3H]³⁺ (monoisotopic *m/z* =

1000.8). This glycopeptide was an attractive model analyte for our initial studies because, as discussed below, the MS/MS behavior of this analyte has been well-studied by others in the past (particularly, with respect to the complementarity of vibrational activation methods and electron capture / transfer methods for glycopeptide analysis). The ion was quadrupole selected and subjected to CID at a variety of collision energies. As shown in **Figure 2.1a-b**, at a collision energy of $\Delta U = 17.5$ V the CID spectrum is dominated by Y-type glycosidic cleavages of the carbohydrate moiety. Sequential loss of individual monosaccharides occurred in various orders, ultimately resulting in a major fragment ion which corresponded to the $Y_{1\alpha}+Y_{1\beta}$ double cleavage product (*i.e.*, the peptide group plus a single remaining GlcNAc residue linked to the asparagine side chain). Not unexpectedly, the CID spectrum of this glycopeptide ion closely resembled the vibrational activation / dissociation spectra obtained by other researchers using IRMPD,³⁵ ion trap CID,³⁷ and beam-type CID in a Q-TOF.³⁸ It should be pointed out that the studies cited above were conducted on two variants of the target glycopeptide: one in which the residue two positions N-terminal of the glycosylation site was isoleucine, and another in which the isoleucine residue was replaced by a valine residue. Although this substitution of one aliphatic residue for another is unlikely to significantly affect the overall dissociation behavior of these glycopeptide variants, we note here that the present studies have been carried out using the valine-containing variant. In line with expectations, some very dissimilar CID results were obtained at somewhat higher collision energies. As depicted in **Figure 2.1c-d**, at a collision energy of $\Delta U = 37.5$ V the spectrum changed dramatically in both overall appearance and in information content. Under these conditions, the base peak of the CID spectrum remained the $Y_{1\alpha}+Y_{1\beta}$ fragment, although a number of major

ions in the spectrum were assigned as *b*- and *y*-type peptide sequence fragments. The observed product ions resulted in 56.3% sequence coverage for the peptide backbone, owing to six *b* ions and eight *y* ions representing cleavage of nine of the 16 peptide amide

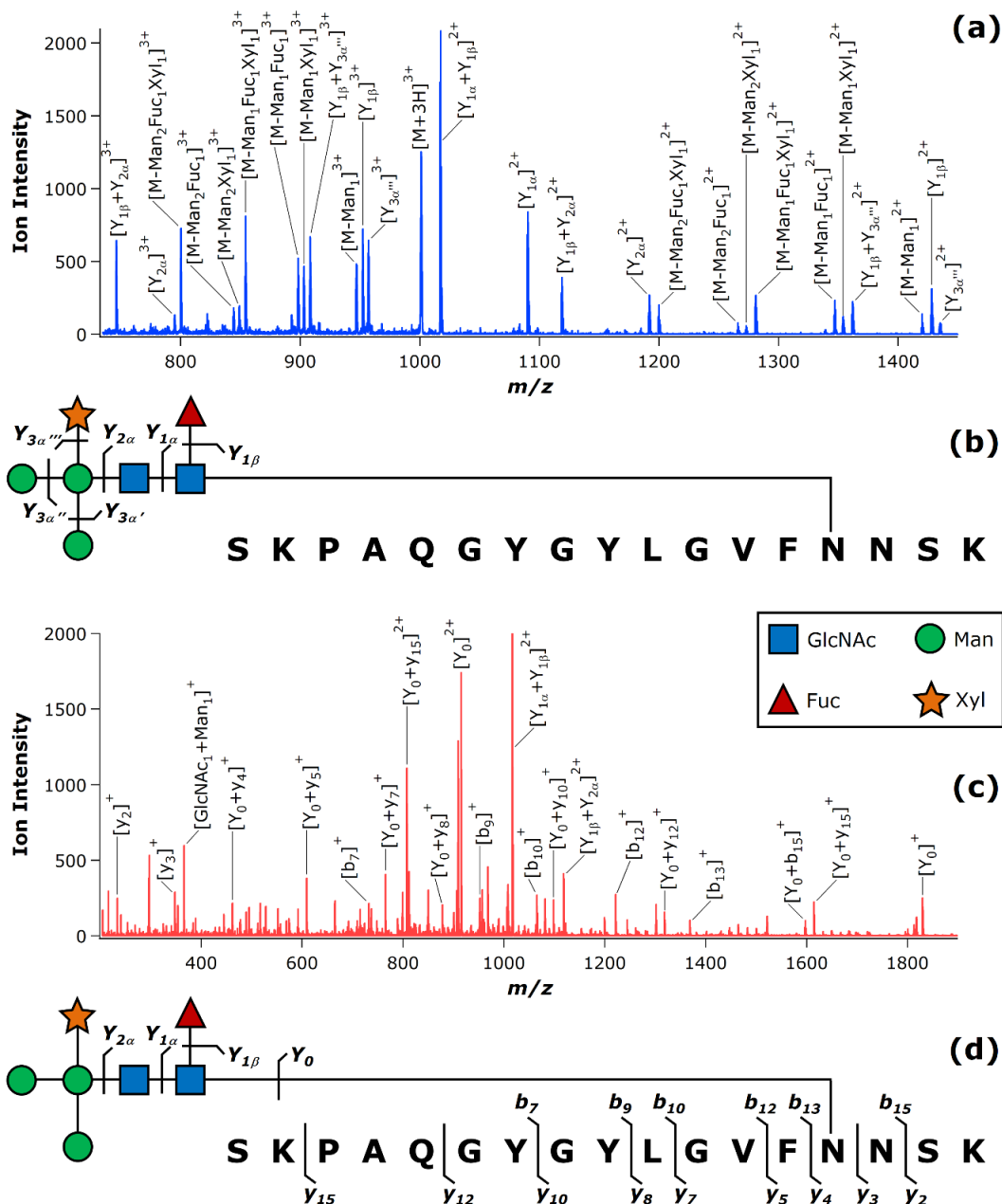


Figure 2.1. CID of the triply protonated ECL glycopeptide. The CID spectrum acquired at $\Delta U = 17.5$ V (a) exhibited only glycan cleavage, as shown in the accompanying diagram (b). The CID spectrum acquired at $\Delta U = 37.5$ V (c) exhibited mainly peptide fragments following glycan loss, as shown in the accompanying diagram (d).

bonds. Notably, the CID sequence coverage reported here is quite reasonable when compared to those previously reported for this glycopeptide ion by ECD or ETD.

Hakansson *et al.* obtained 68.8% sequence coverage by ECD (nine c ions and two z ions representing cleavage of 11 out of 16 N-C $_{\alpha}$ bonds),³⁵ while McLuckey and coworkers achieved 75.0% sequence coverage by ETD (11 c ions and 12 z ions representing cleavage of 12 out of 16 N-C $_{\alpha}$ bonds).³⁸

To more completely delineate the energy-resolved CID behavior of this model glycopeptide, the peak areas of the $[M+3H]^{3+}$ precursor ion and the corresponding product ions (or classes of product ions) were plotted as a function of ΔU (**Figure 2.2**). As the collision energy was increased, the precursor ion was depleted and first yielded an assortment of Y_n glycan fragments, where $n > 1$. The relative proportion of these primary product ions crested at approximately $\Delta U = 17.5$ V, corresponding to the spectrum presented in **Figure 2.1a**. Further increasing the collision energy resulted in diminished

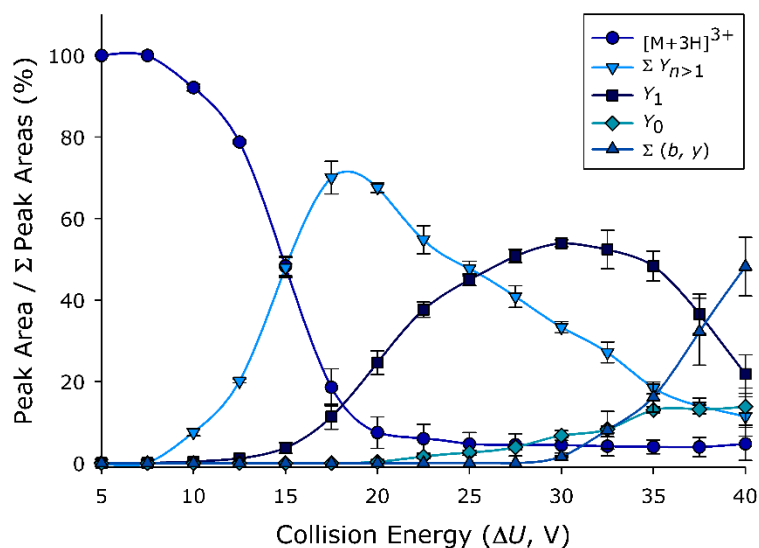


Figure 2.2. Energy-resolved CID plot for the triply protonated ECL glycopeptide. The normalized peak area of each ion or group of ions is plotted as a function of the collision energy, expressed as the applied DC offset. Each data point represents the mean of four replicate measurements; error bars, where visible, represent the standard deviation.

relative abundance of the $Y_{n>1}$ ions, with concomitant increase in proportion of Y_1 fragments, including $Y_{1\alpha}$, $Y_{1\beta}$, and the $Y_{1\alpha} + Y_{1\beta}$ double cleavage product. As the collision energy was elevated to $\Delta U > 32.5$ V, the continued diminution of $Y_{n>1}$ fragments was accompanied by declining abundance of Y_1 fragments. These reductions coincided with the production of a modest fraction of the Y_0 fragment (*i.e.*, loss of the entire oligosaccharide) and a substantial abundance of *b*- and *y*-type peptide fragments. This region of the energy-resolved CID plot corresponds to the spectrum given in **Figure 2.1c**. At $\Delta U = 40.0$ V, peptide *b* and *y* ions accounted for approximately 50% of the integrated peak area of the CID spectrum. Further increasing the collision energy led to loss of ion signal. Overall, these energy-resolved CID results confirm that, while only glycan fragments are yielded *via* the lowest energy dissociation pathways, significant information regarding the peptide sequence can be obtained as later generations of fragment ions evolve at higher collision energies.

Because the glycopeptide under investigation included two particularly basic sites (the ϵ amino groups of the two lysine residues), the triply protonated ion discussed above contains one readily mobile proton.^{62, 63} In order to evaluate how the absence of mobile protons would influence the dissociation channels of this model glycopeptide, the doubly protonated ion [SKPAQGYGYLGVFNNNSK + GlcNAc₂ Man₃ Fuc₁ Xyl₁ + 2H]²⁺ (monoisotopic $m/z = 1500.7$) was generated by adding imidazole to the ZIC-HILIC enriched glycopeptide preparation. As illustrated in **Figure 2.3**, the [M+2H]²⁺ precursor ion also yielded CID spectra containing predominantly carbohydrate *Y* fragments (**Figure 2.3a-b**) at lower collision energies (in this example, $\Delta U = 47.5$ V), while relatively high collision energies (in this example, $\Delta U = 65.0$ V) brought about glycan loss with

subsequent fragmentation of the polypeptide chain (**Figure 2.3c-d**). In comparing the product ion spectra of the $[M+2H]^{2+}$ ion (*i.e.*, with only partially mobile protons) to those of the $[M+3H]^{3+}$ ion (*i.e.*, with one readily mobile proton), it was found that, at

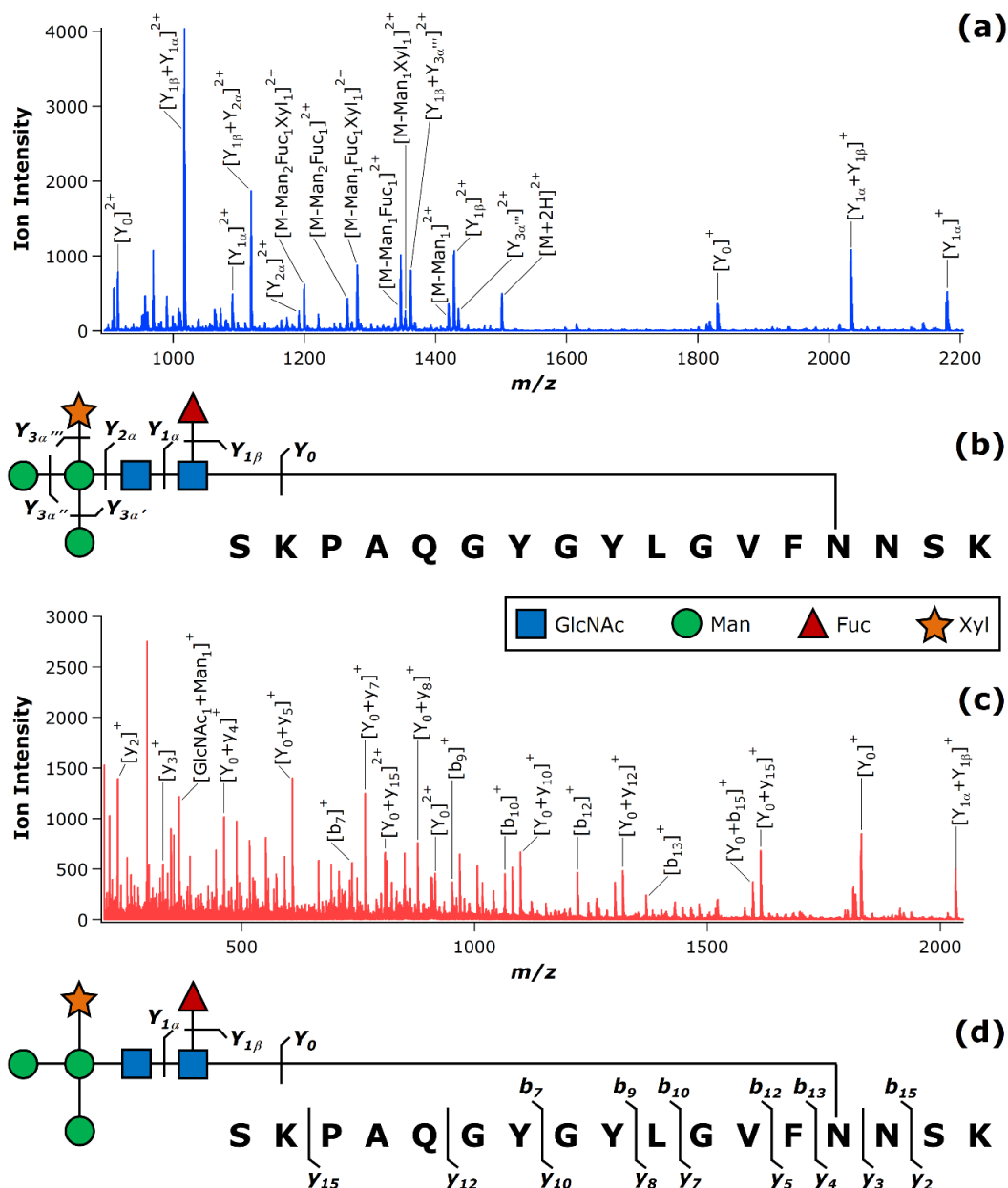


Figure 2.3. CID of the doubly protonated ECL glycopeptide. The CID spectrum acquired at $\Delta U = 47.5$ V (**a**) exhibited only glycan cleavage, as shown in the accompanying diagram (**b**). The CID spectrum acquired at $\Delta U = 65.0$ V (**c**) exhibited mainly peptide fragments following glycan loss, as shown in the accompanying diagram (**d**).

appropriately chosen collision energies, the two precursors were able to yield much the same sequence information. The fragments providing the glycan connectivity were equivalently informative for both precursor ion charge states at the relatively low values of ΔU , and the same peptide sequence coverage was obtained at the relatively high values of ΔU . For the doubly charged precursor, the sequence coverage of 56.3% was obtained on the basis of six b ions and nine y ions. Although the two charge states of this glycopeptide were able to supply similarly revealing CID spectra, not unexpectedly they did so at quite different settings of ΔU . The energy-resolved CID plot for the doubly charged precursor ion (**Figure 2.4**) was generated in the same manner as for the triply charged precursor ion. Although shifted to higher energies, the same general behavior was observed wherein $Y_{n>1}$ fragments of the oligosaccharide were the first fragments to appear, and as the collision energy was increased these fragments gave way to the Y_1 carbohydrate fragments followed by Y_0 glycan loss and finally b and y fragmentation of

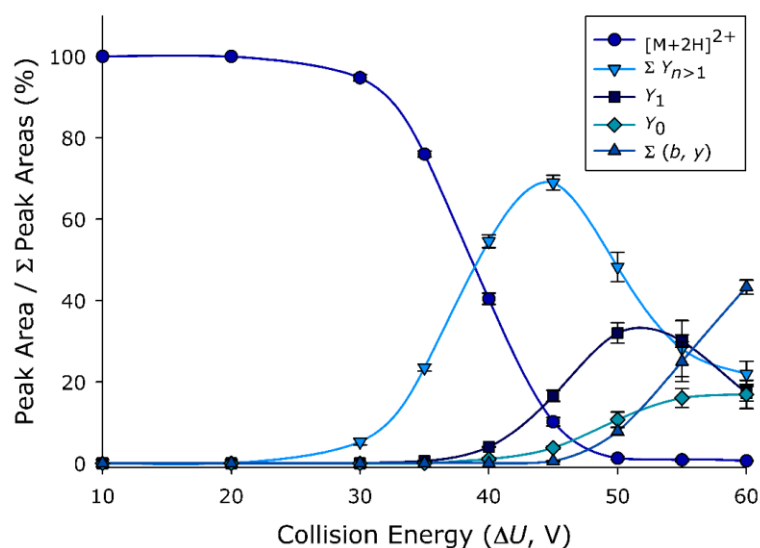


Figure 2.4. Energy-resolved CID plot for the doubly protonated ECL glycopeptide. The normalized peak area of each ion or group of ions is plotted as a function of the collision energy, expressed as the applied DC offset. Each data point represents the mean of three replicate measurements; error bars, where visible, represent the standard deviation.

the peptide chain. It is important to note that the increases in ΔU values necessary to access the various fragmentation pathways was not solely due to differences in ion kinetic energy prior to collision. Applying a linear fit to the inflection point regions of the precursor ion survival curves allowed calculation of the ΔU values which corresponded to depletion of half the precursor ion signal. These 50% precursor ion survivals occurred at $\Delta U = 14.9$ V for the $[M+3H]^{3+}$ glycopeptide ion and $\Delta U = 38.8$ V for the $[M+2H]^{2+}$ precursor. The precursor ion kinetic energy (E_k) relates to the accelerating potential ΔU according to:

$$E_k = ze\Delta U \quad \text{Equation 2.1}$$

where z is the number of charges and e is the fundamental charge. The initial kinetic energies resulting in 50% precursor ion survival were therefore 44.7 eV for the $[M+3H]^{3+}$ and 77.6 eV for the $[M+2H]^{2+}$ ion. These observations are consistent with the mobile proton model, and serve to reiterate the critical importance of collision energy setting upon the information content of glycopeptide CID spectra, and how dramatically this dependence can vary depending on the charge state.

CID of BRB glycopeptide ions. In order to address whether the dissociation behaviors observed for the ECL glycopeptide might be generally true of other glycopeptides, another model analyte was selected for study. The ZIC-HILIC enriched BRB digest exhibited a number of glycopeptide ion signals on nESI-MS analysis. The various peaks represented the microheterogeneity of the BRB glycosylation site, as well as an assortment of fully and partially tryptic digestion products. Among the most abundant signals was the glycopeptide ion $[SRNLTK + GlcNAc_2 Man_5 + 2H]^{2+}$ (monoisotopic $m/z = 968.6$). This model glycopeptide serves as an interesting contrast to

the ECL glycopeptide, in that they harbor different classes of N-glycans (paucimannosidic in the case of the ECL glycopeptide; high mannose in the case of BRB) and have polypeptide groups of quite different lengths (17 amino acid residues in the case of the ECL glycopeptide; six in the case of the BRB glycopeptide). CID spectra of the $[M+2H]^{2+}$ BRB glycopeptide ion are provided in **Figure 2.5**. Much as was noted for the ECL glycopeptide, at relatively low collision energy only the glycan was cleaved (**Figure 2.5a-b**). Conducting CID at $\Delta U = 30.0$ V generated a complete series of Y-type oligosaccharide fragmentation products, which provided the complete glycan composition for this glycopeptide. This spectrum presented in **Figure 2.5a** was found to be less complex than the analogous spectrum of the ECL glycopeptide (**Figure 2.1a**) owing to the lesser number of monosaccharide masses involved, and the correspondingly fewer possible product ion masses arising from oligosaccharide fragmentation. When CID was performed at $\Delta U = 55.0$ V, the dissociation spectrum became dominated by peptide fragments (**Figure 2.5c-d**). These higher energy dissociation pathways yielded product ions covering 80% of the peptide sequence (three *b* ions and two *y* ion representing cleavage of four out of five peptide amide bonds). These observations reinforce the findings for the ECL glycopeptide, where CID spectra alternately produced glycan fragmentation or peptide fragmentation at depending on the applied collision energies. In one contrast to the ECL glycopeptide, at elevated collision energies the BRB glycopeptide was found to yield cross-ring cleavage of the terminal GlcNAc residue ($^{0,2}X_1$). Furthermore, the BRB glycopeptide exhibited some examples of peptide fragmentation without complete loss of the glycan. For instance, the $^{0,2}X_1+b_5$ and Y_1+b_5 internal fragments were among the most abundant signals in the $\Delta U = 55.0$ V CID

spectrum (**Figure 2.5c**). This highlights the possibility that glycan and peptide dissociation channels may take place concurrently under certain circumstances (*e.g.*, when a particularly favored peptide backbone cleavage is available). Similar findings

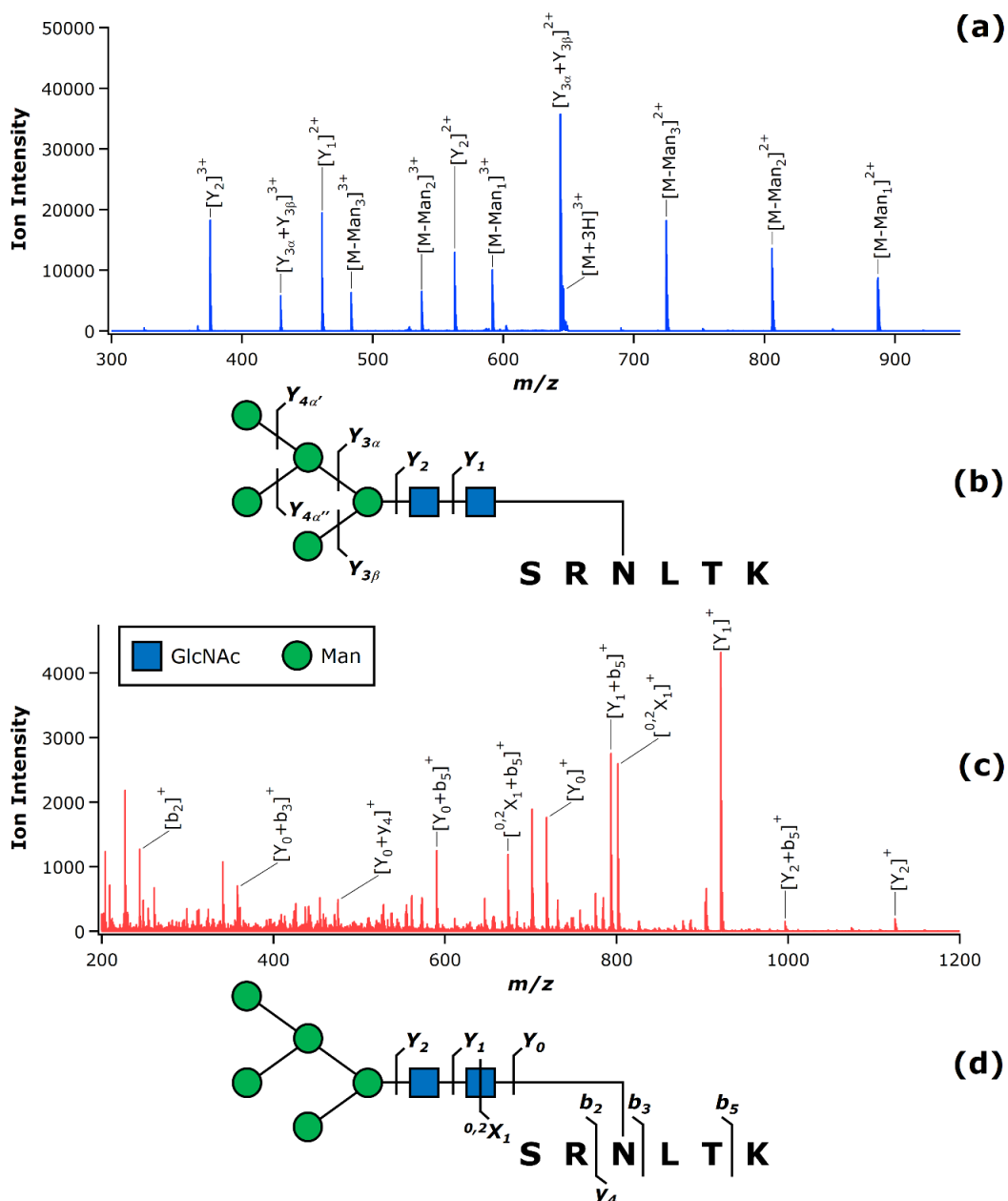


Figure 2.5. CID of the doubly protonated BRB glycopeptide. The CID spectrum acquired at $\Delta U = 30.0$ V (**a**) exhibited only glycan cleavage, as shown in the accompanying diagram (**b**). The CID spectrum acquired at $\Delta U = 55.0$ V (**c**) exhibited mainly peptide fragments following glycan loss, as shown in the accompanying diagram (**d**).

have previously been noted in vibrational activation / dissociation of O-glycopeptides containing proline residues.^{27, 64} In those instances, the proline effect⁶⁵⁻⁶⁷ rendered peptide fragmentation competitive with glycan loss.

The energy-resolved CID behavior of the doubly protonated BRB glycopeptide is presented in **Figure 2.6**. On comparison to the triply protonated ECL glycopeptide ion (**Figure 2.2**), the onset of dissociation for the triply protonated BRB glycopeptide is occurred at somewhat higher collision energies, with the 50% precursor ion survival being reached at $\Delta U = 26.2$ V (corresponding to $E_k = 52.4$ eV) for the $[M+2H]^{2+}$ BRB glycopeptide, as compared to $\Delta U = 14.9$ V (corresponding to $E_k = 44.7$ eV) for the $[M+3H]^{3+}$ ECL glycopeptide. Such differences were not unexpected, given the presence of a readily mobile proton in the case of the triply protonated ECL glycopeptide ion, and the availability of only partially mobile protons in the case of the doubly protonated BRB glycopeptide ion.

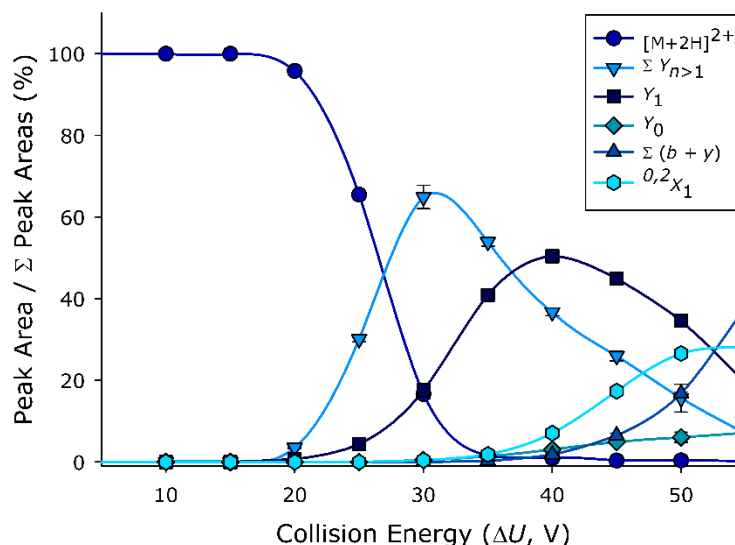


Figure 2.6. Energy-resolved CID plot for the doubly protonated BRB glycopeptide. The normalized peak area of each ion or group of ions is plotted as a function of the collision energy, expressed as the applied DC offset. Each data point represents the mean of three replicate measurements; error bars, where visible, represent the standard deviation.

It should be noted that the substantially different molecular weights of the two glycopeptides (monoisotopic mass of 2999.3 u for the ECL glycopeptide; 1936.2 u for the BRB glycopeptide) and the commensurate disparity in their vibrational degrees of freedom also contributes to quantitative differences in the energy-resolved CID behavior. Aside from the absolute collision energies at which different kinds of dissociation pathways were accessed, the two sets of energy-resolved CID data were in strong agreement regarding the initial appearance of $Y_{n>1}$ glycan fragments followed by Y_1 glycan fragments, which in turn ultimately yielded Y_0 fragment ions (complete glycan loss) and peptide b and y fragment ions. Interestingly, the energy dependences of various dissociation pathways qualitatively mirrored those of the ECL glycopeptide ions. Indeed, these energy-resolved CID data were in strong concordance regarding the initial appearance of $Y_{n>1}$ glycan fragments followed by Y_1 glycan fragments, which in turn ultimately yielded Y_0 fragment ions (complete glycan loss) and peptide b and y fragment ions. These qualitative similarities in the energy-dependent dissociation behavior is rather remarkable, given the significant differences between the glycopeptides in terms of structure and composition.

To again probe the influence of proton mobility on the information content of the CID spectra, the $[\text{SRNLTK} + \text{GlcNAc}_2 \text{Man}_5 + 3\text{H}]^{3+}$ (monoisotopic $m/z = 645.7$) ion was next studied. This ion was observed along with the corresponding doubly charged ion upon nESI-MS analysis of the purified BRB digest, although in less abundance. In contrast to the BRB $[\text{M}+2\text{H}]^{2+}$ ion, this BRB $[\text{M}+3\text{H}]^{3+}$ ion has a number of ionizing protons which exceeds the number of basic amino acid side chains, and thus has a readily mobile proton. As illustrated in **Figure 2.7**, CID at $\Delta U = 10.0$ V produced only Y -type

glycan fragments (**Figure 2.7a-b**), while at $\Delta U = 40.0$ V peptide *b* and *y* ions were observed (**Figure 2.7c-d**). The product ions arising from polypeptide cleavage provided 60% sequence coverage (three *b* ions and one *y* ion representing cleavage of three out of

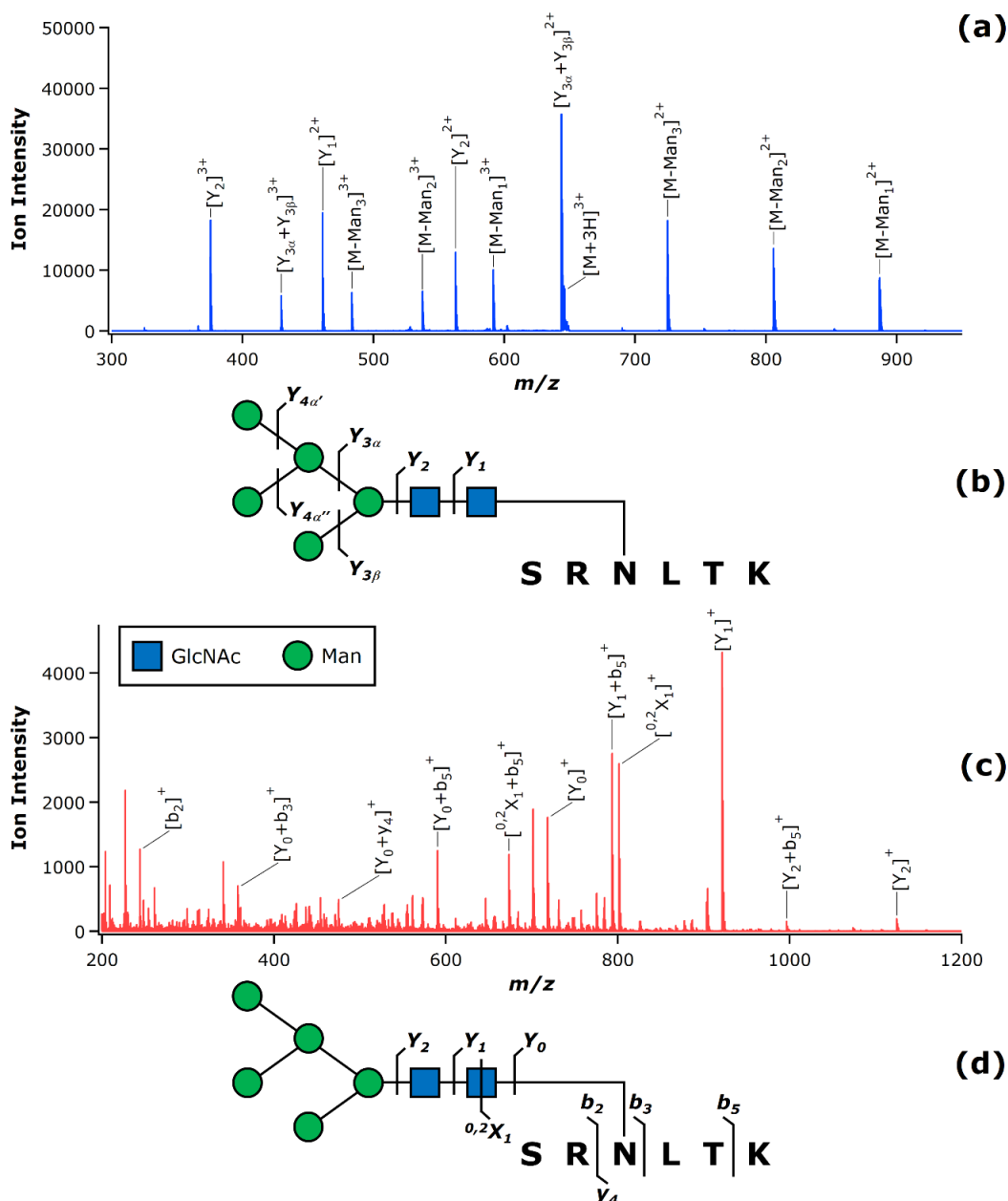


Figure 2.7. CID of the triply protonated BRB glycopeptide. The CID spectrum acquired at $\Delta U = 10.0$ V (**a**) exhibited only glycan cleavage, as shown in the accompanying diagram (**b**). The CID spectrum acquired at $\Delta U = 40.0$ V (**c**) exhibited mainly peptide fragments following glycan loss, as shown in the accompanying diagram (**d**).

five peptide bonds). Predictably, the energy-resolved CID plot for the triply protonated BRB precursor ion exhibited lower dissociation onset energies as compared to the doubly protonated precursor, owing to both the differing charge states (and thus different dependence of E_k upon ΔU) as well as the differences in proton mobility (**Figure 2.8**). These considerations notwithstanding, the general observation that glycan connectivity and peptide sequence can be differentially accessed at different collision energies again held true for this precursor ion.

Multi-energy CID of the ECL and BRB glycopeptides. The energy-resolved CID data discussed above served to suggest the intriguing possibility of capturing oligosaccharide and polypeptide sequence information in a single mass spectrum. In order to achieve this, online collision energy modulation was applied during direct infusion acquisition of CID spectra in order to sample informative dissociation channels

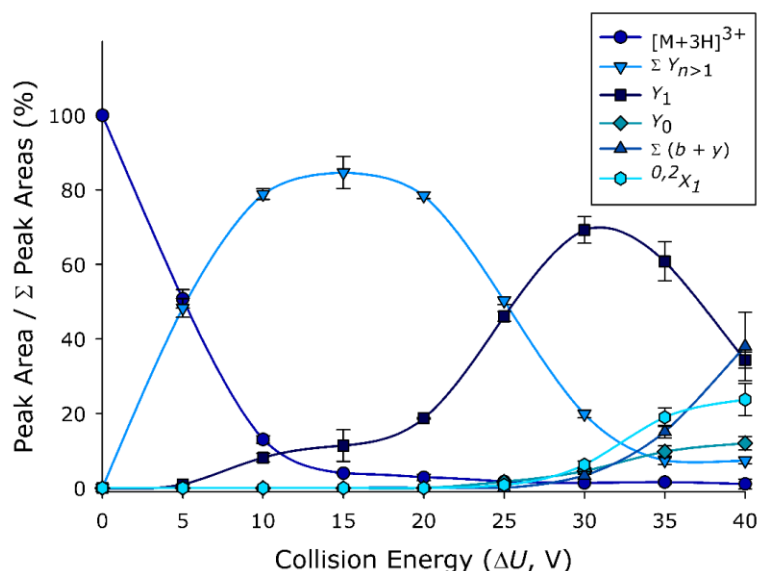


Figure 2.8. Energy-resolved CID plot for the triply protonated BRB glycopeptide. The normalized peak area of each ion or group of ions is plotted as a function of the collision energy, expressed as the applied DC offset. Each data point represents the mean of three replicate measurements; error bars, where visible, represent the standard deviation.

of different energetic requirements. The multi-energy CID spectrum of the $[M+3H]^{3+}$ ECL glycopeptide ion is presented in **Figure 2.9**. The spectrum exhibited a wealth of product ions which collectively resulted in complete coverage of the glycan Y -type ions and 56% peptide sequence coverage (six b ions and nine y ions accounting for scission of nine of the 16 peptide amide bonds). The multi-energy CID spectrum for the $[M+2H]^{2+}$ ECL glycopeptide ion (**Figure 2.10**) provided essentially the same information content. Also noteworthy is that the multi-energy CID spectra obtained through online collision energy modulation compare favorably to the dissociation spectra obtained at a single collision energy (*cf.* **Figure 2.1b**, **Figure 2.1d**, and **Figure 2.9b**). Similarly, multi-energy CID of the $[M+2H]^{2+}$ BRB glycopeptide (**Figure 2.11**) was revealing of a complete series of Y -type glycosidic cleavages as well as 80% peptide sequence coverage. Again,

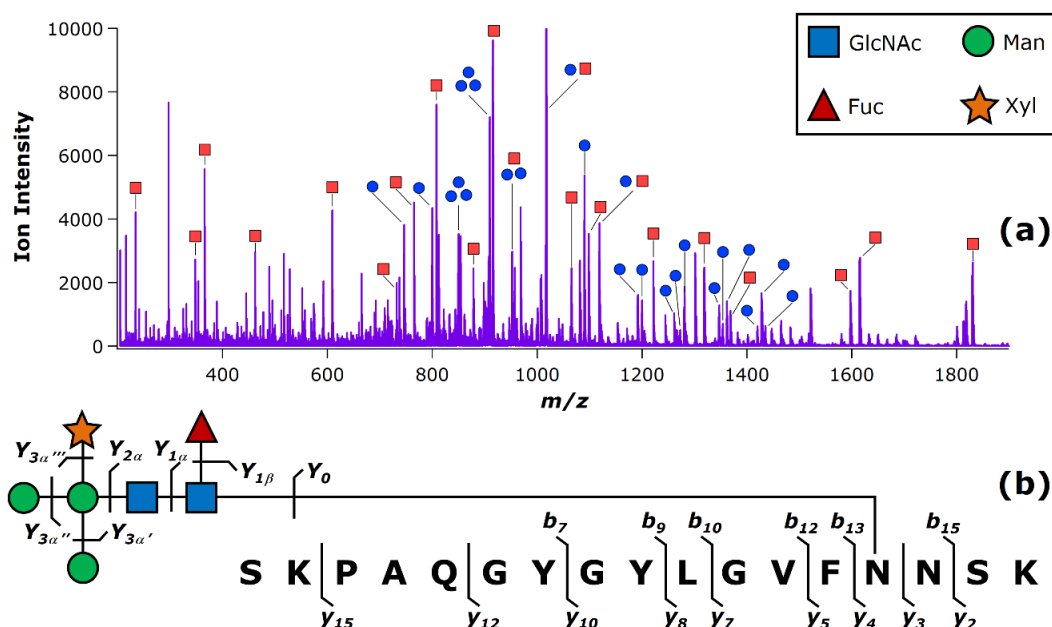


Figure 2.9. Multi-energy CID of the triply protonated ECL glycopeptide. The CID spectrum (a) was acquired via online switching between two collision energies: $\Delta U = 17.5$ V and $\Delta U = 37.5$ V. These correspond to the collision energies applied in **Figure 2.1a** and **Figure 2.1c**, respectively. Peak assignments are the same as those shown in **Figure 2.1a** (labeled here with blue circles) and **Figure 2.1c** (labeled here with red squares). An abundance of both glycan and peptide fragments were observed, as shown in the accompanying diagram (b).

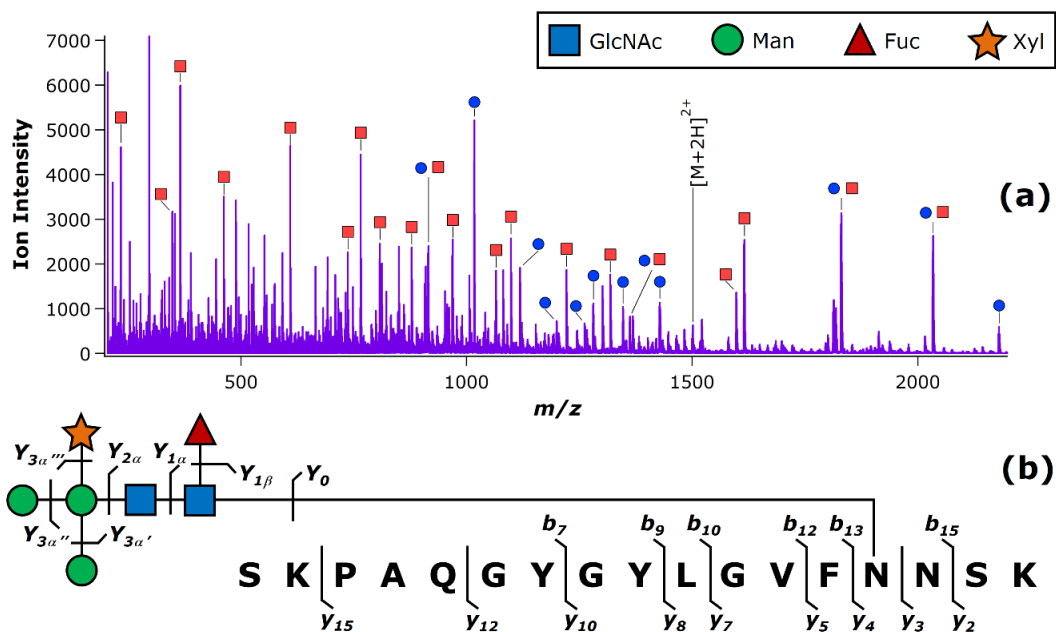


Figure 2.10. Multi-energy CID of the doubly protonated ECL glycopeptide. The CID spectrum (a) was acquired via online switching between two collision energies: $\Delta U = 47.5$ V and $\Delta U = 65.0$ V. These correspond to the collision energies applied in **Figure 2.3a** and **Figure 2.3c**, respectively. Peak assignments are the same as those shown in **Figure 2.3a** (labeled here with blue circles) and **Figure 2.3c** (labeled here with red squares). An abundance of both glycan and peptide fragments were observed, as shown in the accompanying diagram (b).

comparable connectivity information was obtained upon multi-energy CID analysis of an alternative charge state of the analyte (in this case, the $[M+3H]^{3+}$ BRB glycopeptide ion; **Figure 2.12**). Furthermore, the multi-energy CID results for the BRB glycopeptide were found to be of approximately equivalent information content as was achieved in the individual, static collision energy spectra (*cf.*, **Figure 2.5b**, **Figure 2.5d**, and **Figure 2.11b**). Overall, the modulation of collision energy without interrupting spectrum acquisition was found to be a viable approach to obtaining highly informative CID spectra which address the structures of both the glycan and peptide moieties.

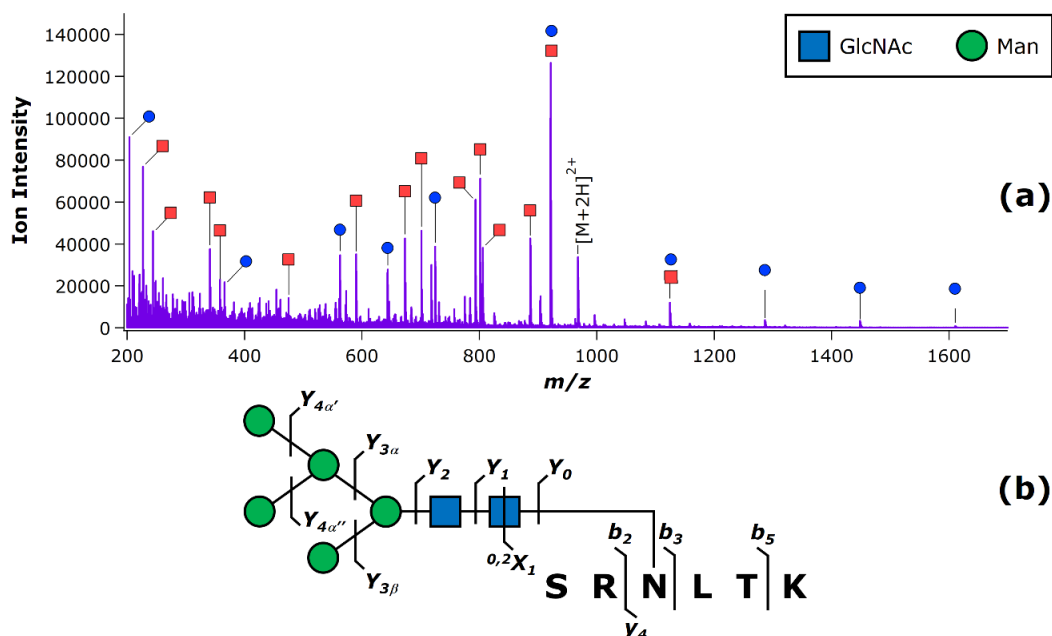


Figure 2.11. Multi-energy CID of the doubly protonated BRB glycopeptide. The CID spectrum (a) was acquired via online switching between two collision energies: $\Delta U = 30.0$ V and $\Delta U = 55.0$ V. These correspond to the collision energies applied in **Figure 2.5a** and **Figure 2.5c**, respectively. Peak assignments are the same as those shown in **Figure 2.5a** (labeled here with blue circles) and **Figure 2.5c** (labeled here with red squares). An abundance of both glycan and peptide fragments were observed, as shown in the accompanying diagram (b).

Conclusions

Although vibrational activation / dissociation MS/MS methods are perhaps best known for the ability to provide information on the carbohydrate moiety of glycopeptides, these data underscore and extend previous observations that, at appropriately chosen collision energies, substantial peptide sequence information can be obtained *via* low-energy beam-type CID. This was found to be true of four model glycopeptide ions which were quite dissimilar in a number of other respects (glycan type and composition; peptide size and composition), and were each investigated as protonated ions having charge states that provided differing proton mobilities. Despite these variables, the analyte ions studied herein adhered to strikingly similar energy-

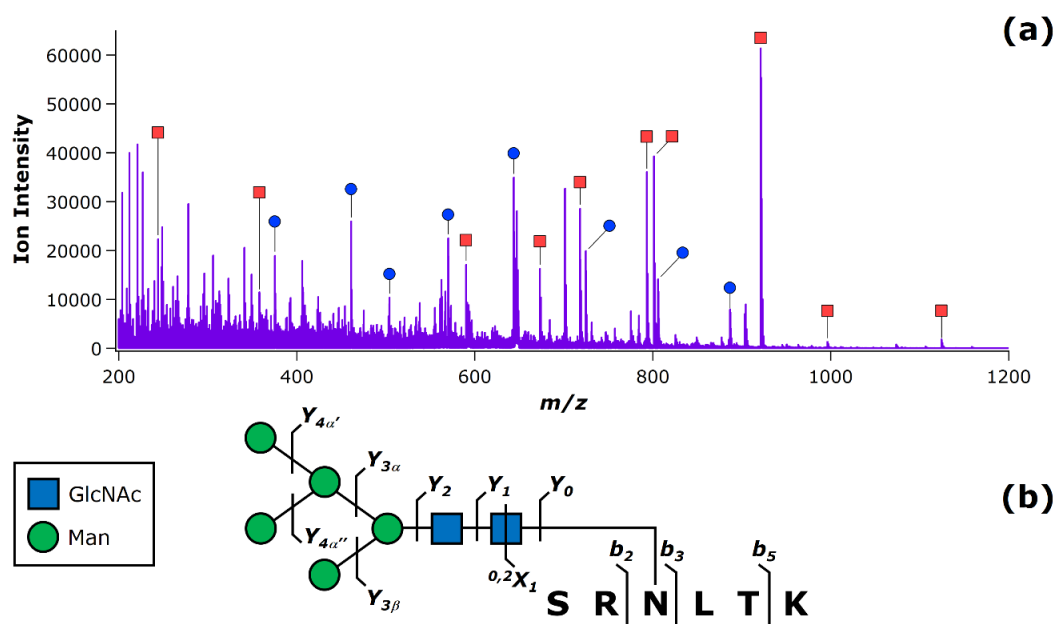


Figure 2.12. Multi-energy CID of the triply protonated BRB glycopeptide. The CID spectrum (a) was acquired via online switching between two collision energies: $\Delta U = 10.0$ V and $\Delta U = 40.0$ V. These correspond to the collision energies applied in **Figure 2.7a** and **Figure 2.7c**, respectively. Peak assignments are the same as those shown in **Figure 2.7a** (labeled here with blue circles) and **Figure 2.7c** (labeled here with red squares). An abundance of both glycan and peptide fragments were observed, as shown in the accompanying diagram (b).

resolved CID behaviors from a qualitative standpoint. In each case, $Y_{n>1}$ carbohydrate cleavage was observed as the lowest-energy, first generation dissociation pathway. With increasing collision energy, production of the Y_1 glycan fragment was observed, which in turn gave rise to the Y_0 product along with b and y ions. Based on the energy-resolved CID precursor and product ion abundance curves, the peptide b and y ions appear to be tertiary fragments which, accordingly, have much higher appearance energy thresholds as compared to the glycan-related scissions. Our findings in aggregate serve to suggest that these dissociation behaviors may be quite general among a diverse range of glycosylated peptides bearing different glycan classes and various peptide characteristics.

The higher energy required to access peptide-informative dissociation channels may in part explain why such ions are sometimes not observed. For example, low-energy CID in an ion trap would not be expected to yield consecutive fragmentation in single MS/MS experiment, since this method only imparts translational energy to the precursor ion. Likewise, IRMPD may in some cases be too slow an activation process to provide extensive peptide sequence information, even though IRMPD is in principle capable of accessing consecutive dissociation products. Although the present findings may be of less usefulness in conjunction with these “slow heating”⁶⁸ vibrational activation methods, they can be of immediate analytical utility when analysis is carried out using any low-energy, beam-type CID instrument, such as tandem quadrupoles, quadrupole time-of-flight hybrids, and various other hybrid mass spectrometers which enable beam-type collisional activation. This includes “higher-energy collisional dissociation” (HCD), which is merely a vendor-specific implementation and terminology for low-energy beam-type CID.

While qualitatively quite similar, there were some important quantitative differences in the energy-resolved CID data among the model glycopeptide ions investigated here. Clearly, the composition, charge state, and proton mobility of the precursor ion exert great influence on the absolute collision energies at which various classes of dissociation products are observed. Accordingly, the ability to collect both glycan and peptide information in a multi-energy CID spectrum hinges upon appropriate selection of the applied ΔU values. Thus, further study of the energy dependence of glycopeptide fragmentation pathways seems warranted. In this respect, some theoretical progress has been made towards predicting glycopeptide tandem mass spectra on the

basis of a kinetic model; however, thus far this has only been performed from the standpoint of ion trap CID under conditions which would not be expected to lead to peptide sequence information.⁶⁹ We are currently pursuing this line of inquiry from an experimental standpoint. Based on energy-resolved CID studies of families of glycopeptides with key differences in composition and charge state, we find that the general conclusions of the present study extend to numerous other glycopeptide analytes, and further that it may be possible to predict collision energies that result in specific fragment types (indeed, the charge state and degrees of freedom corrected 50% precursor ion survival energies seem to correlate well with proton mobility (*Table 2.1*)).

Table 2.1. CID collision energies (ΔU) corresponding to 50% precursor ion survival, and the corresponding precursor ion charge states (z) and vibrational degrees of freedom (f). The charge state and degrees of freedom corrected 50% precursor ion survival energies are given in the rightmost column, and have each been multiplied by a factor of 100 to yield more convenient figures. Within the glycopeptide compositions, amino acid residues with basic side chains are shown in bold, while the glycosylated asparagine residue is underlined. The number of charge-carrying protons (n_{H^+}) are also indicated relative to the number of basic amino acid side chains (n_B).

Glycopeptide Composition	z	f	ΔU (V)	$(z\Delta U/f)$ *100
$n_{H^+} > n_B$ [SKPAQGYGYLGVFNN K +GlcNAc ₂ Man ₃ Xyl ₁ Fuc ₁ +3H] ³⁺	3	1230	14.9	3.63
[<u>SRNLTK</u> +GlcNAc ₂ Man ₅ +3H] ³⁺	3	804	5.5	2.05
$n_{H^+} = n_B$ [SKPAQGYGYLGVFNN K +GlcNAc ₂ Man ₃ Xyl ₁ Fuc ₁ +2H] ²⁺	2	1227	38.8	6.32
[<u>SRNLTK</u> +GlcNAc ₂ Man ₅ +2H] ²⁺	2	801	26.2	6.54

Finally, we note that the development of an enhanced understanding of how CID yields peptide information is quite significant given that the alternatives for this task - ECD and ETD - are not as widely available on as eclectic an array of MS instruments as

compared to CID. Thus, there is potential for substantial impact of these findings in the context of glycoproteomics. The major advantage of ETD is that the peptide backbone can be fragmented without elimination of the glycan, thus allowing unambiguous and direct assignment of the site of modification. However, in many cases involving N-glycosylation, loss of the glycan does not preclude site localization owing to the specificity of N-glycan attachment to only asparagine residues within the context of NXT or NXT consensus sequon (where X is any amino acid residue except proline). For tryptic N-glycopeptides which contain only one potential N-glycosylation site, glycan loss at the stage of MS/MS does not pose a significant limitation for site localization. Moreover, we note that modulating ΔU values to capture spectra at different collision energies can be done in a matter of a few milliseconds, making this approach at least as fast (and potentially faster) than online switching to ETD. This presents an advantage from the standpoint of sampling LC-MS peaks. Overall, these results indicate the possibility of some generally applicable principles of energy-resolved glycopeptide ion CID behaviors of glycosylated peptide ions, while concomitantly underscoring the need for further study of the absolute collision energies necessary to access desired types of fragmentation information. The accomplishment of these goals would undoubtedly bring considerable analytical benefits to the field of glycoproteomics with regards to maximizing the structural information content of glycopeptide CID spectra.

References

1. Dalpathado, D. S.; Desaire, H. *Analyst* **2008**, *133*, 731-738.
2. An, H. J.; J. W. Froehlich, J. W.; Lebrilla, C. B. *Current Opinion in Chemical Biology* **2009**, *13*, 421-426.
3. Tissot, B.; North, S. J.; Ceroni, A.; Pang, P. C.; Panico, M.; Rosati, F.; Capone, A.; Haslam, S. M.; Dell, A.; Morris, H. R. *FEBS Letters* **2009**, *583*, 1728-1735.
4. Schiel, J. E. *Analytical and Bioanalytical Chemistry* **2012**, *404*, 1141-1149.
5. Desaire, H. *Molecular & Cellular Proteomics* **2013**, *12*, 893-901.
6. Varki, A. *Glycobiology* **1993**, *3*, 97-130.
7. Dwek, R. A. *Chemical Reviews* **1996**, *96*, 683-720.
8. Ohtsubo, K.; Marth, J. D. *Cell* **2006**, *126*, 855-867.
9. Marklova, E.; Albahri, Z. *Clinica Chimica Acta* **2007**, *385*, 6-20.
10. An, H. J.; Kronewitter, S. R.; de Leoz, M. L. A.; Lebrilla, C. B. *Current Opinion in Chemical Biology* **2009**, *13*, 601-607.
11. Schachter, H.; Freeze, H. H. *Biochimica et Biophysica Acta* **2009**, *1792*, 925-930.
12. Hwang, H.; Zhang, J.; Chung, K. A.; Leverenz, J. B.; Zabetian, C. P.; Peskind, E. R.; Jankovic, J.; Su, Z.; Hancock, A. M.; Pan, C.; Montine, T. J.; Pan, S.; Nutt, J.; Albin, R.; Gearing, M.; Beyer, R. P.; Shi, M.; Zhang, J. *Mass Spectrometry Reviews* **2010**, *29*, 79-125.
13. Sturiale, L.; Barone, R.; Garozzo, D. *Journal of Inherited Metabolic Disease* **2011**, *34*, 891-899.
14. Adamczyk, B.; Tharmalingam, T.; Rudd, P. M. *Biochimica et Biophysica Acta* **2012**, *1820*, 1347-1353.

15. Kolarich, D.; Lepenies, B.; Seeberger, P. H. *Current Opinion in Chemical Biology* **2012**, *16*, 214-220.
16. Kreisman, L. S. C.; Cobb, B. A. *Glycobiology* **2012**, *22*, 1019-1030.
17. Freeze, H. H. *Journal of Biological Chemistry* **2013**, *288*, 6936-6945.
18. Dodds, E. D.; Seipert, R. R.; Clowers, B. H.; German, J. B.; Lebrilla, C. B. *Journal of Proteome Research* **2009**, *8*, 502-512.
19. Wuhrer, M.; Deelder, A. M.; Hokke, C. H. *Journal of Chromatography B* **2005**, *825*, 124-133.
20. Morelle, W.; Canis, K.; Chirat, F.; Faid, V.; Michalski, J. C. *Proteomics* **2006**, *6*, 3993-4015.
21. Morelle, W.; Michalski, J. C. *Nature Protocols* **2007**, *2*, 1585-1602.
22. Clowers, B. H.; Dodds, E. D.; Seipert, R. R.; Lebrilla, C. B. *Journal of Proteome Research* **2007**, *6*, 4032-4040.
23. Froehlich, J. W.; Dodds, E. D.; Wilhelm, M.; Serang, O.; Steen, J. A.; Lee, R. S. *Molecular & Cellular Proteomics* **2013**, *12*, 1017-1025.
24. Froehlich, J. W.; Barboza, M.; Chu, C.; Lerno, Jr., L. A.; Clowers, B. H.; Zivkovic, A. M.; German, J. B.; Lebrilla, C. B. *Analytical Chemistry* **2011**, *83*, 5541-5547.
25. Vekey, K.; Ozohanics, O.; Toth, E.; Jeko, A.; Revesz, A.; Krenyacz, J.; Drahos, L. *International Journal of Mass Spectrometry* **2013**, *345-347*, 71-79.
26. Seipert, R. R.; Dodds, E. D.; Clowers, B. H.; Beecroft, S. M.; German, J. B.; Lebrilla, C. B. *Analytical Chemistry* **2008**, *80*, 3684-3692.

27. Seipert, R. R.; Dodds, E. D.; Lebrilla, C. B. *Journal of Proteome Research* **2009**, *8*, 493-501.
28. Yoshimura, Y.; Matsushita, T.; Fujitani, N.; Takegawa, Y.; Fujihira, H.; Naruchi, K.; Gao, X. D.; Manri, N.; Sakamoto, T.; Kato, K.; Hinou, H.; Nishimura, S.I. *Biochemistry* **2010**, *49*, 5929-5941.
29. Manri, N.; Satake, H.; Kaneko, A.; Hirabayashi, A.; Baba, T.; Sakamoto, T. *Analytical Chemistry* **2013**, *85*, 2056-2063.
30. Zhu, Z.; Hua, D.; Clark, D. F.; Go, E. P.; Desaire, H. *Analytical Chemistry* **2013**, *85*, 5023-5032.
31. Zhu, Z.; Su, X.; Clark, D. F.; Go, E. P.; Desaire, H. *Analytical Chemistry* **2013**, *85*, 8403-8411.
32. Zhang, L.; Reilly, J. P. *Journal of Proteome Research* **2008**, *8*, 734-742.
33. Madsen, J. A.; Ko, B. J.; Xu, H.; Iwashkiw, J. A.; Robotham, S. A.; Shaw, J. B.; Feldman, M. F.; Brodbelt, J. S. *Analytical Chemistry* **2013**, *85*, 9253-9261.
34. Mirgorodskaya, E.; Roepstorff, P.; Zubarev, R. A. *Analytical Chemistry* **1999**, *71*, 4431-4436.
35. Hakansson, K.; Cooper, H. J.; Emmett, M. R.; Costello, C. E.; Marshall, A. G.; Nilsson, C. L. *Analytical Chemistry* **2001**, *73*, 4530-4536.
36. Hakansson, K.; Chalmers, M. J.; Quinn, J. P.; McFarland, M. A.; Hendrickson, C. L.; Marshall, A. G. *Analytical Chemistry* **2003**, *75*, 3256-3262.
37. Hogan, J. M.; Pitteri, S. J.; Chrisman, P. A.; McLuckey, S. A. *Journal of Proteome Research* **2005**, *4*, 628-632.

38. Han, H.; Xia, Y.; Yang, M.; McLuckey, S. A. *Analytical Chemistry* **2008**, *80*, 3492-3497.
39. Halim, A.; Nilsson, J.; Ruetschi, U.; Hesse, C.; Larson, G. *Molecular & Cellular Proteomics* **2012**, *11*, 1-17.
40. Halim, A.; Ruetschi, U.; Larson, G.; Nilsson, J. *Journal of Proteome Research* **2013**, *12*, 573-584.
41. Singh, C.; Zampronio, C. G.; Creese, A. J.; Cooper, H. J. *Journal of Proteome Research* **2012**, *11*, 4517-4525.
42. Wang, D.; Hincapie, M.; Rejtar, T.; Karger, B. L. *Analytical Chemistry* **2011**, *83*, 2029-2037.
43. Ye, H.; Boyne, M. T.; Buhse, L. F.; Hill, J. *Analytical Chemistry* **2013**, *85*, 1531-1539.
44. Wuhrer, M.; Catalina, M. I.; Deelder, A. M.; Hokke, C. H. *Journal of Chromatography B* **2007**, *849*, 115-128.
45. Zaia, J. *Omics* **2010**, *14*, 401-418.
46. Dodds, E. D. *Mass Spectrometry Reviews* **2012**, *31*, 666-682.
47. Alley, Jr., W. R.; Mann, B. F.; Novotny, M. V. *Chemical Reviews* **2013**, *113*, 2668-2732.
48. Adamson, J. T.; Hakansson, K. *Journal of Proteome Research* **2006**, *5*, 493-501.
49. Bindila, L.; Steiner, K.; Schaffer, C.; Messner, P.; Mormann, M.; Peter-Katalinic, J. *Analytical Chemistry* **2007**, *79*, 3271-3279.
50. Bykova, N. V.; Rampitsch, C.; Krokhin, O.; Standing, K. G.; Ens, W. *Analytical Chemistry* **2006**, *78*, 1093-1103.

51. Damen, C. W.; Chen, W.; Chakraborty, A. B.; van Oosterhout, M.; Mazzeo, J. R.; Gebler, J. C.; Schellens, J. H.; Rosing, H.; Beijnen, J. H. *Journal of the American Society for Mass Spectrometry* **2009**, *20*, 2021-2033.
52. Krokhin, O.; Ens, W.; Standing, K. G.; Wilkins, J.; Perreault, H. *Rapid Communications in Mass Spectrometry* **2004**, *18*, 2020-2030.
53. Segu, Z. M.; Mechref, Y. *Rapid Communications in Mass Spectrometry* **2010**, *24*, 1217-1225.
54. Scott, N. E.; Parker, B. L.; Connolly, A. M.; Paulech, J.; Edwards, A. V. G.; Crossett, B.; Falconer, L.; Kolarich, D.; Djordjevic, S. P.; Hojrup, P.; Packer, N. H.; Larsen, M. R.; Cordwell, S. J. *Molecular & Cellular Proteomics* **2011**, *10*, 1-18.
55. Irungu, J.; Go, E. P.; Zhang, Y.; Dalpathado, D. S.; Liao, H. X.; Haynes, B. F.; Desaire, H. *Journal of the American Society for Mass Spectrometry* **2008**, *19*, 1209-1220.
56. Jahouh, F.; Hou, S. J.; Kovac, P.; Banoub, J. H. *Journal of Mass Spectrometry* **2011**, *46*, 993-1003.
57. Franc, V.; Sebela, M.; Rehulka, P.; Koncitikova, R.; Lenobel, R.; Madzak, C.; Kopecny, D. *Journal of Proteomics* **2012**, *75*, 4027-4037.
58. Tajiri, M.; Kadoya, M.; Wada, Y. *Journal of Proteome Research* **2009**, *8*, 688-693.
59. Domon, B.; Costello, C. E. *Glycoconjugate Journal* **1988**, *5*, 397-409.
60. Roepstorff, P.; Fohlman, J. *Biomedical Mass Spectrometry* **1984**, *11*, 601.

61. Varki, A.; Cummings, R. D.; Esko, J. D.; Freeze, H. H.; Stanley, P.; Marth, J. D.; Bertozzi, C. R.; Hart, G. W.; Etzler, M. E. *Proteomics* **2009**, *9*, 5398-5399.
62. Dongre, A. R.; Jones, J. L.; Somogyi, A.; Wysocki, V. H. *Journal of the American Chemical Society* **1996**, *118*, 8365-8374.
63. Wysocki, V. H.; Tsaprailis, G.; Smith, L. L.; Brechi, L. A. *Journal of Mass Spectrometry* **2000**, *35*, 1399-1406.
64. Perdivara, I.; Perera, L.; Sricholpech, M.; Terajima, M.; Pleshko, N.; Yamauchi, M.; Tomer, K. B. *Journal of the American Society for Mass Spectrometry* **2013**, *24*, 1072-1081.
65. Brechi, L. A.; Tabb, D. L.; Yates, J. R.; Wysocki, V. H. *Analytical Chemistry* **2003**, *75*, 1963-1971.
66. Paizs, B.; Suhai, S. *Mass Spectrometry Reviews* **2005**, *24*, 508-548.
67. Huang, Y.; Tseng, G. C.; Yuan, S.; Pasa-Tolic, L.; Lipton, M. S.; Smith, R. D.; Wysocki, V. H. *Journal of Proteome Research* **2008**, *7*, 70-79.
68. McLuckey, S. A.; Goeringer, D. E. *Journal of Mass Spectrometry* **1997**, *32*, 461-474.
69. Zhang, Z.; Shah, B. *Analytical Chemistry* **2010**, *82*, 10194-10202.

Chapter 3

The Role of Proton Mobility in Determining the Energy-Resolved Vibrational Activation / Dissociation Channels of N-Glycopeptide Ions

Portions of this chapter will appear in:

V. Kolli, H. A. Roth, G. De La Cruz, G. S. Fernando, and E. D. Dodds (submitted).

Abstract

Site-specific glycoproteomic analysis largely hinges on the use of tandem mass spectrometry (MS/MS) to identify glycopeptides. Experiments of this type are usually aimed at drawing connections between specific oligosaccharide structures and their specific sites of attachment to the polypeptide chain. These determinations inherently require ion dissociation methods capable of interrogating both the monosaccharide and amino acid connectivity of the glycopeptide. Collision-induced dissociation (CID) shows potential to satisfy this requirement, as the vibrational activation / dissociation of protonated N-glycopeptides has been observed to access cleavage of either glycosidic bonds of the glycan or amide bonds of the peptide in an energy-resolved manner. Nevertheless, the relative energy requirement for these fragmentation pathways varies considerably among analytes. This research addresses the influence of proton mobility on the vibrational energy necessary to achieve either glycan or peptide cleavage in a collection of protonated N-glycopeptide ions. While greater proton mobility of the precursor ion was found to correlate with lower energy requirements for precursor ion depletion and appearance of glycosidic fragments, the vibrational energy deposition necessary for appearance of peptide backbone fragments showed no relation to the precursor ion proton mobility. These results are consistent with previous observations suggesting that peptide fragments arise from an intermediate fragment which is generally of lower proton mobility than the precursor ion. Such findings have potential to facilitate the rational selection of CID conditions which are best suited to provide either glycan or peptide cleavage products in MS/MS based glycoproteomic analysis.

Introduction

Mass spectrometry (MS) based glycoproteomics is an emerging branch of post-genomic analytical science that lies at the intersection of proteomics and glycomics.¹⁻⁴ While glycoproteomic experiments are conducted with widely varied scopes and objectives, they are generally aimed at the identification or characterization of glycosylated proteins; the compositional or structural determination of protein-linked oligosaccharides; and the association of individual oligosaccharide compositions or structures with specific sites of attachment to the protein.⁵⁻⁸ Accordingly, a wide assortment of MS centered tools are actively applied to glycoproteomics.⁹⁻¹² In many of these approaches, tandem mass spectrometry (MS/MS) of glycosylated proteolytic fragments plays a critical role, often serving as the final analytical readout of the experiment.¹³⁻¹⁴

Although MS/MS analysis of glycopeptides is analytically demanding (polypeptide sequence and oligosaccharide connectivity are simultaneously involved), these experiments can provide a level of molecular detail not afforded by methods which release the glycan from the protein prior to analysis.¹⁵⁻¹⁶ Nevertheless, complete elucidation of glycopeptide topology requires MS/MS methods capable of providing information on both the amino acid sequence and the monosaccharide connectivity. While this is frequently accomplished by combining multiple, complementary ion fragmentation methods,¹³⁻¹⁴ several such methods have been shown capable of probing both the oligosaccharide and polypeptide moieties of glycopeptides. These include ultraviolet photodissociation (UVPD),¹⁷⁻¹⁸ infrared multiphoton dissociation (IRMPD),¹⁹⁻²² and low-energy beam-type collision-induced dissociation (CID).²³⁻²⁶

By a wide margin, CID is the most widely available ion dissociation method for MS/MS. While a disadvantage of CID is loss of the glycan prior to the onset of peptide fragmentation, in most cases this does not hinder the localization of N-glycosylation, which only occurs within the context of a consensus sequon (multiple instances of which rarely appear on the same proteolytic fragment). Therefore, extending the applicability of CID for N-glycopeptide analysis is of significant interest. One barrier towards an expanded role for CID in glycoproteomics is that the distinct energetic requirements for accessing glycosidic bond cleavages or peptide backbone cleavages are not well understood in terms of the physicochemical characteristics of the precursor ions.²⁷⁻²⁸

The present work is focused on the relationship between precursor ion proton mobility²⁹⁻³⁰ and optimum collision energies for accessing glycan versus peptide scission. Energy-resolved CID studies were conducted on a group of protonated N-glycopeptides in which different amino acid compositions and charge states were represented. In general, precursor ion proton mobility correlated negatively with the collision energies necessary to deplete the precursor ion and provide glycosidic cleavage; however, the collision energies needed to achieve peptide fragmentation had no noticeable relationship to the proton mobility of the precursor ion. This is consistent with energy-resolved CID results that show the peptide fragmentation products arise from an intermediate fragment of low proton mobility. On the whole, these findings suggest that, with adequate knowledge of the relevant fragmentation processes, CID could be conducted such that the monosaccharide connectivity and amino acid sequence of protonated N-glycopeptides are deliberately accessed.

Materials and Methods

Reagents and materials. Ammonium bicarbonate, bovine ribonuclease B (BRB), dithiothreitol, formic acid, imidazole, iodoacetamide, proteomics grade trypsin, and urea were all procured from Sigma-Aldrich (St. Louis, MO, USA). Acetonitrile (HPLC grade) and water (HPLC grade) were obtained from Fisher Scientific (Fair Lawn, NJ, USA) and Burdick & Jackson (Muskegon, MI, USA), respectively. Zwitterionic hydrophilic interaction liquid chromatography (ZIC-HILIC) micropipette tips for solid phase extraction (SPE) were acquired from Protea Biosciences (Somerset, NJ, USA).

Glycopeptide preparation. A 50 μL aliquot of 2 $\mu\text{g}/\mu\text{L}$ BRB glycoprotein solution in 8 M urea and 50 mM NH_4HCO_3 (pH 7.5) was subjected to disulfide bond reduction by addition of 10 μL of 450 mM dithiothreitol in 50 mM NH_4HCO_3 (pH 7.5; incubated 1 h at 55°C). The sample was next subjected to thiol alkylation by treatment with 10 μL 500 mM iodoacetamide in 50 mM NH_4HCO_3 (pH 7.5; incubated 1 h at room temperature and in the dark). A fresh portion (175 μL) of 50 mM NH_4HCO_3 (pH 7.5) was added to the reduced and alkylated glycoprotein sample such that the total urea concentration was reduced to < 2 M. Proteolysis was then performed through addition of a 5 μL aliquot of 0.5 $\mu\text{g}/\mu\text{L}$ of trypsin (incubated 18 h at 37°C). The resulting tryptic digest was reduced to ~ 10 μL in volume *via* vacuum centrifugation (Speed Vac SC110, Thermo Savant, Holbrook, NY, USA), then reconstituted in 0.1% HCOOH to a final volume of ~ 100 μL . Glycopeptides from an aliquot of this solution (4 μL reconstituted digest diluted to a total volume of 20 μL with CH_3CN) were enriched and purified using ZIC-HILIC SPE. Briefly, the SPE micropipette tip was equilibrated with 80% CH_3CN / 0.1% HCOOH, loaded with the sample aliquot described above, washed with 80%

CH₃CN / 0.1% HCOOH, and finally eluted in 20 μ L 0.1% HCOOH. In some cases, purified digests were spiked to contain 10 mM imidazole. This was done in order to enhance the production of glycopeptide ions with lower charge states for study.

Mass spectrometry and data analysis. The purified glycopeptide digest was prepared for MS analysis by placing a portion of ZIC-HILIC SPE eluate (~ 5-10 μ L) into a home-pulled glass emitter for nanoelectrospray ionization (nESI). This transfer was accomplished using a Hamilton 10 μ L taper-tipped syringe (Reno, NV, USA). The nESI emitters were prepared from 1.5 - 1.8 x 100 mm melting point capillary tubes (Corning Pyrex, Corning, NY, USA) with the aid of a vertical micropipette puller (David Kopf Instruments, Tujunga, CA, USA). The filled emitter was then fitted to a custom-built holder which made use of a platinum wire to provide the nESI potential directly to the analyte solution. This apparatus was then adapted onto the commercial nESI source of a Waters Synapt G2 HDMS quadrupole time of flight (Q-TOF) hybrid mass spectrometer (Manchester, UK). Ion source conditions for nESI included an emitter potential of 1.0 - 1.4 kV, a sampling cone potential of 15 - 35 V, an extraction cone potential of 2 - 4 V, and a temperature of 80°C. For MS/MS experiments, quadrupole selection of precursor ions was followed by CID in the “trap” region of the instrument (a stacked ring ion guide containing argon at a pressure of approximately 5.0 x 10⁻³ mbar). The DC offset (ΔU) which determined the kinetic energy of ions entering the collision cell was systematically adjusted in order to obtain energy-resolved CID spectra.

All instrument control and data acquisition was conducted with the use of MassLynx 4.1 (Waters). Subsequent data handling and graph generation was performed using IGOR Pro 6.3 (WaveMetrics, Lake Oswego, OR, USA) and SigmaPlot 10.1

(Systat, Chicago, IL, USA). For schematic purposes, standard one-letter amino acid abbreviations were used in diagramming the peptide moiety, while glycan structures were diagrammed using the conventions suggested by Varki *et al.*³¹ The assignment of fragment ions was performed in accord with the formalisms of Domon and Costello (for glycan fragments) and Roepstorff and Fohlman (for peptide fragments).³²⁻³³ In accord with these systems of nomenclature, lower case letters were used to indicate peptide fragments, while upper case letters were used to indicate glycan fragments. If multiple glycan cleavages (or combinations thereof) could plausibly yield a given product ion mass, the fragment ion was assigned by indicating the composition of losses from the precursor ion (*e.g.*, [M - Man₂]²⁺). For simplicity, small neutral losses from precursor or fragment ions (*e.g.*, NH₃, H₂O) were not labeled in the spectra. Monosaccharide names were abbreviated as follows: GlcNAc, N-acetylglucosamine; Man, mannose.

Results and Discussion

Overview. As described above, a set of model glycopeptide analytes was prepared by trypsinolysis of BRB with the goal of quantitatively characterizing the influence of proton mobility upon the energy-resolved vibrational activation / dissociation pathways of selected N-glycopeptides. The presence of several potential tryptic cleavage sites in close proximity to the single glycosylation site of BRB, coupled with the tendency of glycosylation to sterically interfere with protease action,³⁴⁻³⁷ resulted in the production of glycopeptides with multiple amino acid sequences based on a combination of the fully tryptic cleavage product and various partially tryptic cleavage products. Specifically, N-glycopeptides with the amino acid sequences NLTK, NLTKDR, SRNLTK, and

SRNLTKDR were obtained. This provided a group of model glycopeptide analytes which encompassed some key variations in sequence, particularly with respect to the number and location of basic sites. Protonated glycopeptide ions based on the above peptide groups carrying the GlcNAc₂Man₅ high mannose N-glycan were each studied in two charge states by energy-resolved CID, as described in detail below.

Precursor ion survival curves. MS/MS data were collected *via* CID for each of eight glycopeptide precursor ions: NLTK + GlcNAc₂Man₅ as the [M+H]⁺ and [M+2H]²⁺ ions; NLTKDR + GlcNAc₂Man₅ as the [M+2H]²⁺ and [M+3H]³⁺ ions; SRNLTK + GlcNAc₂Man₅ as the [M+2H]²⁺ and [M+3H]³⁺ ions; and SRNLTKDR + GlcNAc₂Man₅ as the [M+2H]²⁺ and [M+3H]³⁺ ions. In these experiments, CID was conducted at various applied ΔU values, which were adjusted in 2.5 – 10.0 V increments, depending on the analyte. The resulting spectra were used to prepare precursor ion survival curves by plotting the percent fractional area of the precursor ion peak as a function of the applied collision energy. As depicted in **Figure 3.1**, this relatively small set of related glycopeptide precursor ions (*i.e.*, all bearing the same glycan composition, and all derived from the same glycosylation site) exhibited a remarkably broad range of energy-dependent stabilities, with the applied ΔU resulting in < 20% precursor ion survival ranging from approximately 10.0 V – 60.0 V. This underscores a key challenge in the interrogation of glycopeptide connectivity by CID; namely, the selection of collision energies yielding CID spectra which are most informative of the overall topology of a given glycopeptide precursor ion. This is particularly important given the ability of vibrational activation / dissociation methods to provide fragments which can be

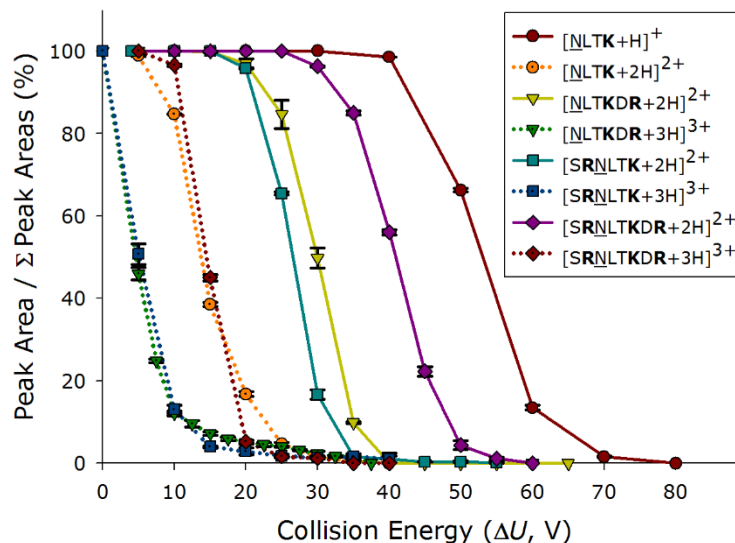


Figure 3.1. Precursor ion survival curves for each of the glycopeptide ions studied. The sequences of the peptide moieties and overall ion charge states are given in the inset. In addition, each glycopeptide harbored the GlcNAc₂Man₅ N-glycan. Amino acid residues with basic side chains are shown in bold, while the glycosylated asparagine residue is underlined. Each data point represents the mean of three replicate measurements; error bars, where visible, represent the standard deviation.

informative of either the oligosaccharide connectivity or the polypeptide sequence, depending on the amount of vibrational energy deposited.²⁵⁻²⁶

While **Figure 3.1** is useful in illustrating the highly varied degrees of precursor ion depletion as a function of ΔU (*i.e.*, the instrumental parameter which is most directly used to determine the amount of vibrational energy deposited into the precursor ion), comparisons between the stabilities of the various precursor ions are difficult to rationalize from visual inspection of these data alone. Indeed, the precursor ion survival behaviors are dictated by not only the compositions of the analyte ions, but also their charge states and number of vibrational degrees of freedom.³⁸⁻³⁹ To allow more meaningful comparisons among the various analytes studied, the initial kinetic energies which resulted in 50% depletion of the precursor were calculated and normalized for the number of vibrational modes available to the analyte. This was carried out by first

applying a linear fit to the steepest region of each precursor ion survival curve, then determining value of ΔU which corresponded to 50% fractional intensity of the precursor ion. These values were in turn used to calculate the corresponding initial kinetic energy, E_k , (expressed with units of eV) of the precursor ion using **Equation 3.1**:

$$E_k = z\Delta U \quad \text{Equation 3.1}$$

Here, z represents the precursor ion charge state expressed as an integer multiple of the fundamental charge. These values, which account for the charge state of the precursor ion, were further normalized for the number of vibrational degrees of freedom, f_v , available to the precursor ion. For an analyte composed of n atoms:

$$f_v = 3n - 6 \quad \text{Equation 3.2}$$

The vibrational degrees of freedom normalized initial precursor ion kinetic energy, $E_{k,n}$, was then defined and calculated according to:

$$E_{k,n} = \frac{10^2 E_k}{f_v} \quad \text{Equation 3.3}$$

where the factor of 10^2 was applied to provide more convenient values for comparison (thus, the values of $E_{k,n}$ are 10^2 times the number of electron volts per vibrational mode).

The values of $E_{k,n}$ corresponding to the 50% survivals of all precursor ions studied are provided in **Table 3.1**.

In general, the vibrational energy deposition required to deplete 50% of the initial precursor ion population was found to negatively correlate with proton mobility, as estimated based on the relative number of charge-carrying protons (n_H) and basic amino acid residues (n_B) present. For each precursor ion studied here, the charge-carrying proton(s) could be described as “mobile,” “partially mobile,” or “nonmobile.” These

Table 3.1. Potential differences (ΔU) and degrees of freedom normalized initial precursor ion kinetic energies ($E_{k,n}$) resulting in 50% precursor ion survival of each glycopeptide ion studied. The number of charge-carrying protons (n_H) is indicated relative to the number of basic amino acid residues (n_B), and precursor ion charge states (z) and vibrational degrees of freedom (f_v) are given. Within the glycopeptide compositions, basic amino acid residues are bolded, and the glycosylated asparagine residue is underlined. The “cleavage intensity ratio” (CIR) is also provided for each precursor ion according to Kapp *et al.*⁴⁰ Larger CIR values indicate lower proton mobility, as estimated based upon the precursor ion charge state and amino acid composition.

		50% Precursor Ion Survival				
Glycopeptide Composition		CIR	z	f_v	ΔU	$E_{k,n}$
$n_H > n_B$	[<u>N</u> LT K +GlcNAc ₂ Man ₅ +2H] ²⁺	0.73	2	693	14.5	4.18
	[<u>S</u> R <u>N</u> LT K +GlcNAc ₂ Man ₅ +3H] ³⁺	0.90	3	804	5.5	2.05
	[<u>N</u> LT KDR +GlcNAc ₂ Man ₅ +3H] ³⁺	0.90	3	810	3.9	1.44
$n_H = n_B$	[<u>N</u> LT K +GlcNAc ₂ Man ₅ +H] ⁺	2.18	1	690	52.2	7.57
	[<u>S</u> R <u>N</u> LT K +GlcNAc ₂ Man ₅ +2H] ²⁺	1.56	2	801	26.2	6.54
	[<u>N</u> LT KDR +GlcNAc ₂ Man ₅ +2H] ²⁺	1.56	2	807	29.8	7.39
	[<u>S</u> R <u>N</u> LT KDR +GlcNAc ₂ Man ₅ +3H] ³⁺	1.52	3	900	14.9	4.97
$n_H < n_B$	[<u>S</u> R <u>N</u> LT KDR +GlcNAc ₂ Man ₅ +2H] ²⁺	4.58	2	897	41.0	9.14

categories, suggested by Kapp *et al.*, were based on empirically determined “cleavage intensity ratios” (CIRs) determined according to the relative proportion of fragmentation products known to be enhanced in the absence of mobile protons.⁴⁰ Those authors used the prevalence of such fragments as an indicator of proton mobility for a large number of peptides studied by CID. Accordingly, CIR values increase with decreasing proton mobility. In the present experiments, glycopeptide precursor ions with $n_H > n_B$, which thus contained a readily mobile proton (with CIRs ranging from 0.73 – 0.90), exhibited 50% precursor ion survivals at $E_{k,n}$ values ranging from 1.44 – 4.18. For glycopeptide ions with $n_H = n_B$, thus rendering the protons partially mobile (with CIRs ranging from 1.52 – 2.18), the $E_{k,n}$ values corresponding to 50% precursor ion survival were significantly higher on average, ranging from 4.97 – 7.57. Finally, one analyte in which

all protons were considered nonmobile (CIR of 4.58) had a 50% precursor ion survival occurring at an $E_{k,n}$ value of 9.14. Taken together, these data demonstrate that the order of charge state corrected and vibrational degrees of freedom normalized initial precursor ion kinetic energies which brought about 50% precursor ion depletion can be rationalized by proton mobility; that is, those precursor ions characterized by lower proton mobility required greater vibrational energy deposition per vibrational mode in order to bring about unimolecular dissociation processes. Nevertheless, the normalized collision energies needed to access an analytically useful degree of precursor ion fragmentation varied substantially within this group of glycopeptides which, in many ways, would be considered quite similar (all derived from the same glycosylation site, and all bearing the same glycan).

Energy-resolved CID comparisons at various proton mobilities. In order to further delineate the role of proton mobility in the vibrational activation / dissociation behavior of glycopeptides, energy-resolved breakdown curves were plotted for each precursor ion under study. At each collision energy, the total peak areas were determined for each of several product ion categories: the precursor ion, $[M+nH]^{n+}$; the larger *Y*-type glycosidic bond cleavage products, $\Sigma Y_{n>1}$; the peptide chain with one remaining GlcNAc residue attached, Y_1 ; the bare peptide chain, Y_0 ; cross-ring cleavage of the reducing terminal GlcNAc residue, 0,2X_0 ; and peptide backbone fragmentation products, $\Sigma(b+y)$. The fraction of the total spectral peak area arising from fragment ions in each of these categories were then plotted against collision energy, expressed as the applied ΔU . In **Figure 3.2**, CID breakdown curves are presented for three representative glycopeptide ions with differing proton mobilities: $[NLTkDR + \text{GlcNAc}_2\text{Man}_5 + 3H]^{3+}$ ($n_H > n_B$);

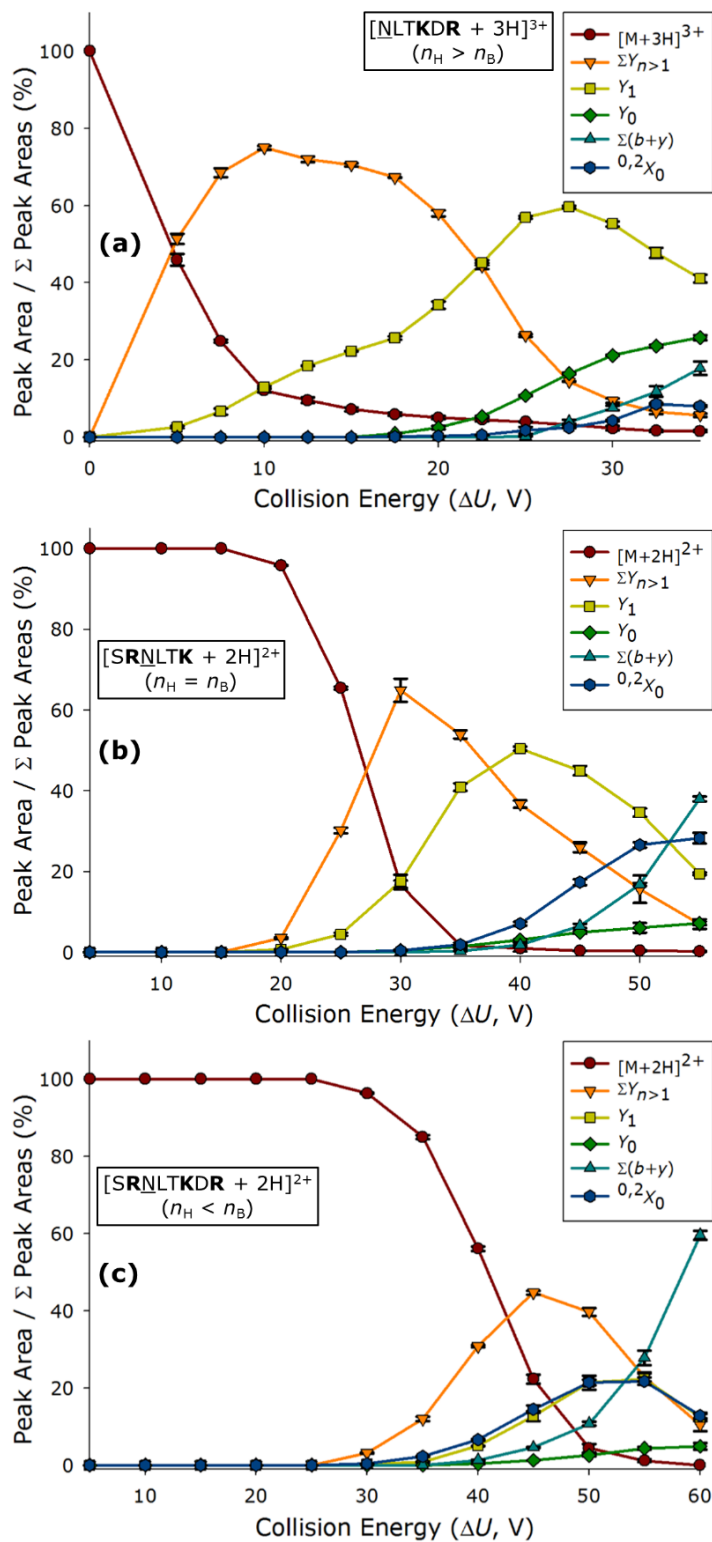


Figure 3.2. Energy-resolved CID breakdown curves for the [NLTKDR + GlcNAc₂Man₅ + 3H]³⁺ (a; $n_H > n_B$), [SRNLTK + GlcNAc₂Man₅ + 2H]²⁺ (b; $n_H = n_B$), and [SRNLTKDR + GlcNAc₂Man₅ + 2H]²⁺ (c; $n_H < n_B$) glycopeptide ions. Additional explanation is provided in the caption to **Figure 3.1**.

[SRNLTK + GlcNAc₂Man₅ + H]²⁺ ($n_H = n_B$); and [SRNLTKDR + GlcNAc₂Man₅ + 2H]²⁺ ($n_H < n_B$). The energy-resolved CID breakdown curves for the remaining glycopeptide ions under study are provided below (**Figures 3.3-3.7**). As we have previously noted of other glycopeptide ions,²⁵⁻²⁶ the energy-resolved CID behaviors of these precursors were found to be qualitatively similar despite significant differences in proton mobility. In each case, the precursor ions first dissociated to give rise to $Y_{n>1}$ glycan fragments. With further increases in vibrational energy deposition, the $Y_{n>1}$ dissociation products gradually gave way to an abundance of Y_1 ions. Finally, at sufficiently high collision energies, a decline in the intensity of Y_1 ions was accompanied by the production of ^{0,2} X_0 , Y_0 , and peptide b and y ions. Indeed, for all of the glycopeptide ions studied here, fragment ions of these various types appeared in the same qualitative order with increasing collision energy. Nevertheless, there are substantial quantitative differences in the energy-resolved CID behaviors of the glycopeptide ions. That is, the specific range of

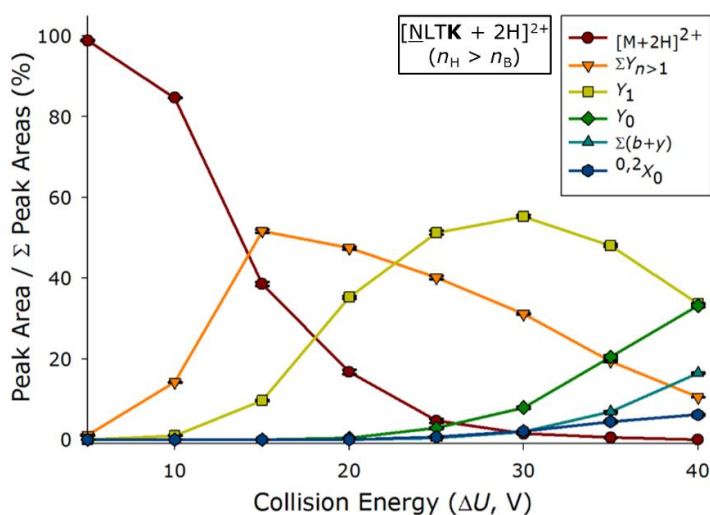


Figure 3.3. Energy-resolved CID breakdown curve for the [NLTK + GlcNAc₂Man₅ + 2H]²⁺ glycopeptide ion. Amino acid residues with basic side chains are shown in bold, while the glycosylated asparagine residue is underlined. Each data point represents the mean of three replicate measurements; error bars, where visible, represent the standard deviation.

ΔU values which yield a given type of fragment ion is widely varied among precursor ions of different proton mobilities.

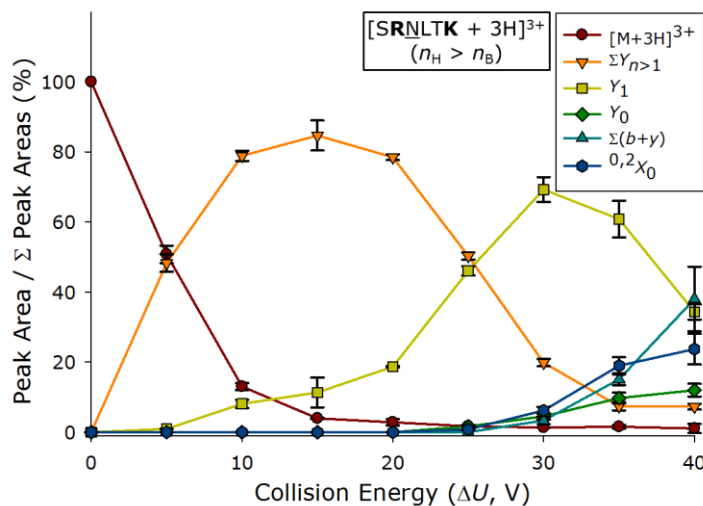


Figure 3.4. Energy-resolved CID breakdown curve for the $[\text{SRNLTK} + \text{GlcNAc}_2\text{Man}_5 + 3\text{H}]^{3+}$ glycopeptide ion. Amino acid residues with basic side chains are shown in bold, while the glycosylated asparagine residue is underlined. Each data point represents the mean of three replicate measurements; error bars, where visible, represent the standard deviation.

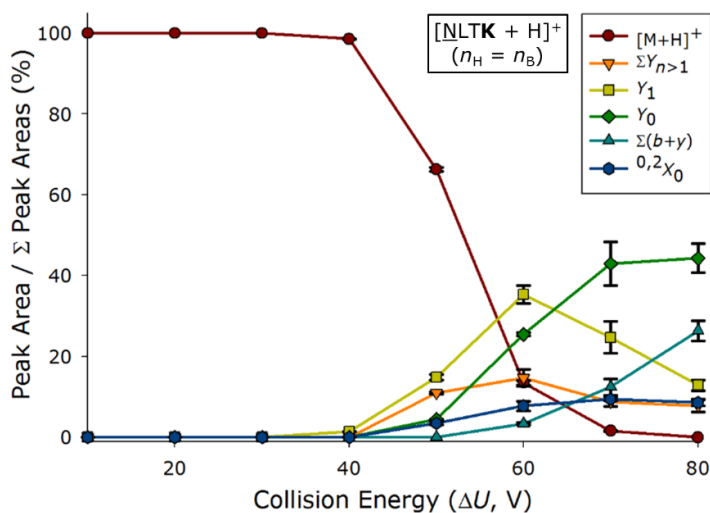


Figure 3.5. Energy-resolved CID breakdown curve for the $[\text{NLTK} + \text{GlcNAc}_2\text{Man}_5 + \text{H}]^+$ glycopeptide ion. Amino acid residues with basic side chains are shown in bold, while the glycosylated asparagine residue is underlined. Each data point represents the mean of three replicate measurements; error bars, where visible, represent the standard deviation.

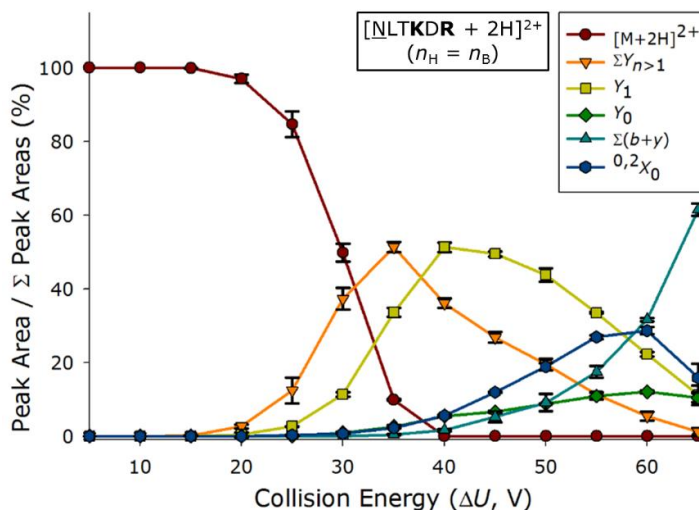


Figure 3.6. Energy-resolved CID breakdown curve for the $[\text{NLTkDR} + \text{GlcNAc}_2\text{Man}_5 + 2\text{H}]^{2+}$ glycopeptide ion. Amino acid residues with basic side chains are shown in bold, while the glycosylated asparagine residue is underlined. Each data point represents the mean of three replicate measurements; error bars, where visible, represent the standard deviation.

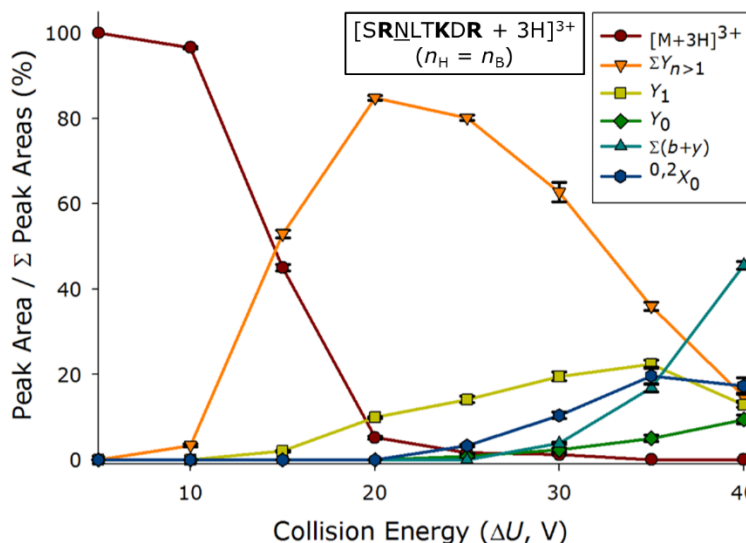


Figure 3.7. Energy-resolved CID breakdown curve for the $[\text{SRNLTkDR} + \text{GlcNAc}_2\text{Man}_5 + 3\text{H}]^{3+}$ glycopeptide ion. Amino acid residues with basic side chains are shown in bold, while the glycosylated asparagine residue is underlined. Each data point represents the mean of three replicate measurements; error bars, where visible, represent the standard deviation.

To provide a means for quantitative comparison of the vibrational energy required to access glycosidic and peptide backbone cleavages, additional $E_{k,n}$ values were

calculated for the corresponding regions of the energy-resolved CID breakdown curves. First, $E_{k,n}$ values which brought about the maximum total intensity of $Y_{n>1}$ glycosidic fragments were determined by fitting the most abundant three to four points of the $\Sigma Y_{n>1}$ curve with a quadratic function (*i.e.*, downward opening parabola), and calculating the inflection point of this function. This was taken to represent the approximate value of ΔU which provided maximum glycosidic fragmentation. Similarly, the ΔU value at which the $\Sigma(b+y)$ peptide fragments first constituted 20% of the total integrated peak area was obtained from a linear fit of the $\Sigma(b+y)$ line in the energy-resolved CID breakdown plot. The 20% intensity was chosen because, while most of the glycopeptides eventually yielded peptide b and y ions to comprise approximately 40% or more of the integrated peak area (*e.g.*, **Figure 3.2b-c**), in two cases only about 20% of the peak area could be attributed to peptide backbone cleavage products (*e.g.*, **Figure 3.2a**). Thus, the 20% peptide fragment appearance value was used to enable reasonable comparisons among the different precursor ions. In the cases of both maximum $\Sigma Y_{n>1}$ intensity and 20% $\Sigma(b+y)$ intensity, the ΔU values of interest were used to calculate the corresponding $E_{k,n}$ values (*cf.* **Equations 1-3**). For each glycopeptide ion under study, these $E_{k,n}$ values are summarized in **Table 3.2**.

Similar to the results for precursor ion survival (*cf.* **Table 3.1**), the $E_{k,n}$ values which yielded maximum $\Sigma Y_{n>1}$ intensity were seen to correlate with the CIR values assigned to each peptide moiety. That is, the $E_{k,n}$ values correlate inversely with proton mobility, as expected. For precursor ions with a readily mobile proton ($n_H > n_B$), $E_{k,n}$ values ranged from 4.74 – 5.56; for precursor ions with a partially mobile proton ($n_H = n_B$), $E_{k,n}$ values ranged from 7.67 – 8.65; and for the precursor ion with no mobile protons

Table 3.2. Potential differences (ΔU) and degrees of freedom normalized initial precursor ion kinetic energies ($E_{k,n}$) resulting in the maximum proportion of glycosidic bond cleavage products ($\sum Y_{n>1}$), and those necessary for peptide backbone cleavage products ($\sum(b,y)$) to constitute 20% of the integrated peak area for each glycopeptide ion. Additional explanation is provided in the caption to **Table 3.1**.

					Max $\sum Y_{n>1}$ Intensity	20% $\sum(b,y)$ Intensity						
Glycopeptide Composition					CIR	z	f_v	ΔU	$E_{k,n}$	ΔU	$E_{k,n}$	
[NLTK+GlcNAc ₂ Man ₅ +2H] ²⁺					0.73	2	693	17.0	4.91	42.9	12.38	
$n_H > n_B$	[SRNLTK+GlcNAc ₂ Man ₅ +3H] ³⁺					0.90	3	804	14.9	5.56	35.3	13.17
	[NLTKDR+GlcNAc ₂ Man ₅ +3H] ³⁺					0.90	3	810	12.8	4.74	35.2	13.04
[NLTK+GlcNAc ₂ Man ₅ +H] ⁺					2.18	1	690	58.8	8.52	75.2	10.90	
$n_H = n_B$	[SRNLTK+GlcNAc ₂ Man ₅ +2H] ²⁺					1.56	2	801	31.3	7.82	49.9	12.46
	[NLTKDR+GlcNAc ₂ Man ₅ +2H] ²⁺					1.56	2	807	34.9	8.65	56.2	13.93
	[SRNLTKDR+GlcNAc ₂ Man ₅ +3H] ³⁺					1.52	3	900	23.0	7.67	34.5	11.50
$n_H < n_B$	[SRNLTKDR+GlcNAc ₂ Man ₅ +2H] ²⁺					4.58	2	897	46.2	10.30	52.4	11.68

($n_H < n_B$), $E_{k,n}$ value was 10.30. This underscores the influence of proton mobility upon the vibrational energy necessary to achieve the highest proportion of glycosidic scission products. Contrastingly, the $E_{k,n}$ values that produced peptide b and y ions with an aggregate of 20% total spectral peak intensity fell in a relatively narrow range. All of these $E_{k,n}$ values ranged from 10.90 – 13.93, with no clear relation to the proton mobility of the precursor ion. While initially unexpected, this can be rationalized by noting that, as illustrated by the energy-resolved CID breakdown curves (**Figure 3.2**), the Y_0 , b , and y ions appear to be tertiary products of sequential fragmentation, arising largely from further fragmentation of the Y_1 ion. This suggests that the vibrational energy required to achieve peptide amide bond scission is not a function of the precursor ion proton

mobility, but dictated by the proton mobility of the Y_l fragment. As these Y_l fragments typically had lower charge states than the precursor ion (as will be shown and further discussed below), their proton mobilities were thus lower than those of the corresponding precursor ions. As a consequence, the vibrational degrees of freedom normalized initial precursor ion kinetic energies that bring about polypeptide b and y ions are quite similar among precursor ions – even those with very dissimilar precursor ion survival energies and glycosidic fragment appearance energies – because in each case the peptide sequence ions originate from an intermediate fragment with no mobile protons. These general observations could eventually be of considerable practical usefulness for the deliberate production of amino acid sequence information for unknown glycopeptides by CID.

CID spectrum comparisons at various proton mobilities. With knowledge of how the precursor ion characteristics of protonated glycopeptides influence their energy-resolved CID behaviors, collision energies could be selected such that information on either the oligosaccharide connectivity or the polypeptide sequence was intentionally accessed. **Figure 3.8** provides the CID spectra of the same representative glycopeptide ions for which energy-resolved CID breakdown curves were shown in **Figure 3.2**. In these spectra, collision energies chosen to approximate the $E_{k,n}$ values corresponding to maximum $\Sigma Y_{n>1}$ intensity (*cf.* **Table 3.2**). In each case, the CID spectra exhibited extensive series of Y -type fragment ions yielding the complete connectivity of the oligosaccharide group, down to at least the Y_l (and in one case, Y_0) ion. In addition to the Y -type dissociation products, a prominent cross-ring cleavage product ($^{0,2}X_0$) was noted in the CID spectrum of the $[\text{SRNLTKDR} + \text{GlcNAc}_2\text{Man}_5 + 2\text{H}]^{2+}$ ion (**Figure 3.8c**). While informative as to the general topology and composition of the glycan, none of these

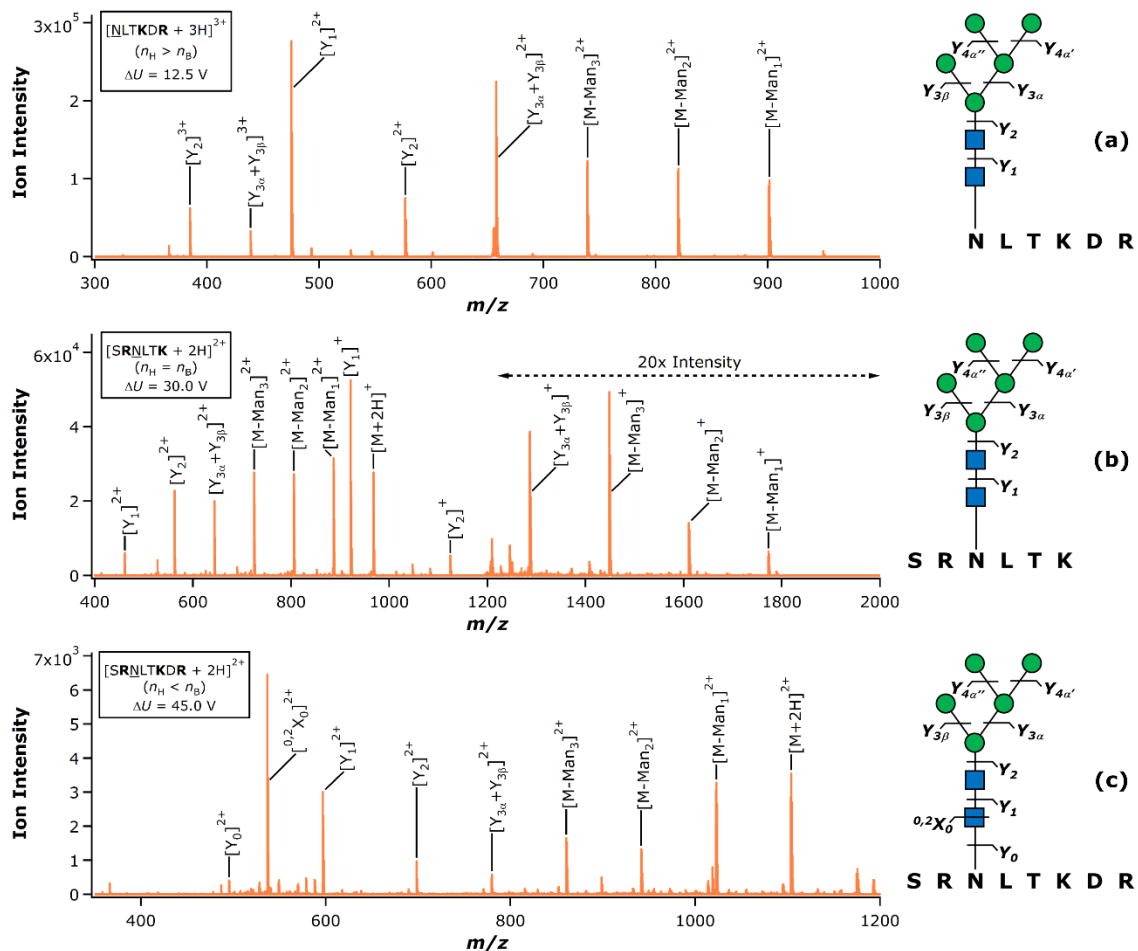


Figure 3.8. CID spectra for the $[\text{NLTKDR} + \text{GlcNAc}_2\text{Man}_5 + 3\text{H}]^{3+}$ (**a**; $n_{\text{H}} > n_{\text{B}}$), $[\text{SRNLTK} + \text{GlcNAc}_2\text{Man}_5 + 2\text{H}]^{2+}$ (**b**; $n_{\text{H}} = n_{\text{B}}$), and $[\text{SRNLTKDR} + \text{GlcNAc}_2\text{Man}_5 + 2\text{H}]^{2+}$ (**c**; $n_{\text{H}} < n_{\text{B}}$). The applied precursor acceleration potentials (ΔU) are indicated, and were chosen to bring about the maximum proportion of glycosidic bond cleavage products (*cf.* **Table 3.2**). Cleavage maps summarizing the fragmentation of each glycopeptide are provided to the right of each spectrum.

spectra were found to yield any detectable peptide backbone fragmentation. The same glycopeptide ions were then interrogated at collision energies consistent with $E_{k,n}$ values known to bring about $\geq 20\% \Sigma(b+y)$ intensity (*cf.* **Table 3.2**); the resulting dissociation spectra are provided in **Figure 3.9**. Under these conditions, each precursor ion could be fragmented to yield significant information on the amino acid connectivity, with the peptide sequence coverages for the $[\text{NLTKDR} + \text{GlcNAc}_2\text{Man}_5 + 3\text{H}]^{3+}$, $[\text{SRNLTK} + \text{GlcNAc}_2\text{Man}_5 + 2\text{H}]^{2+}$, and $[\text{SRNLTKDR} + \text{GlcNAc}_2\text{Man}_5 + 2\text{H}]^{2+}$ glycopeptide ions

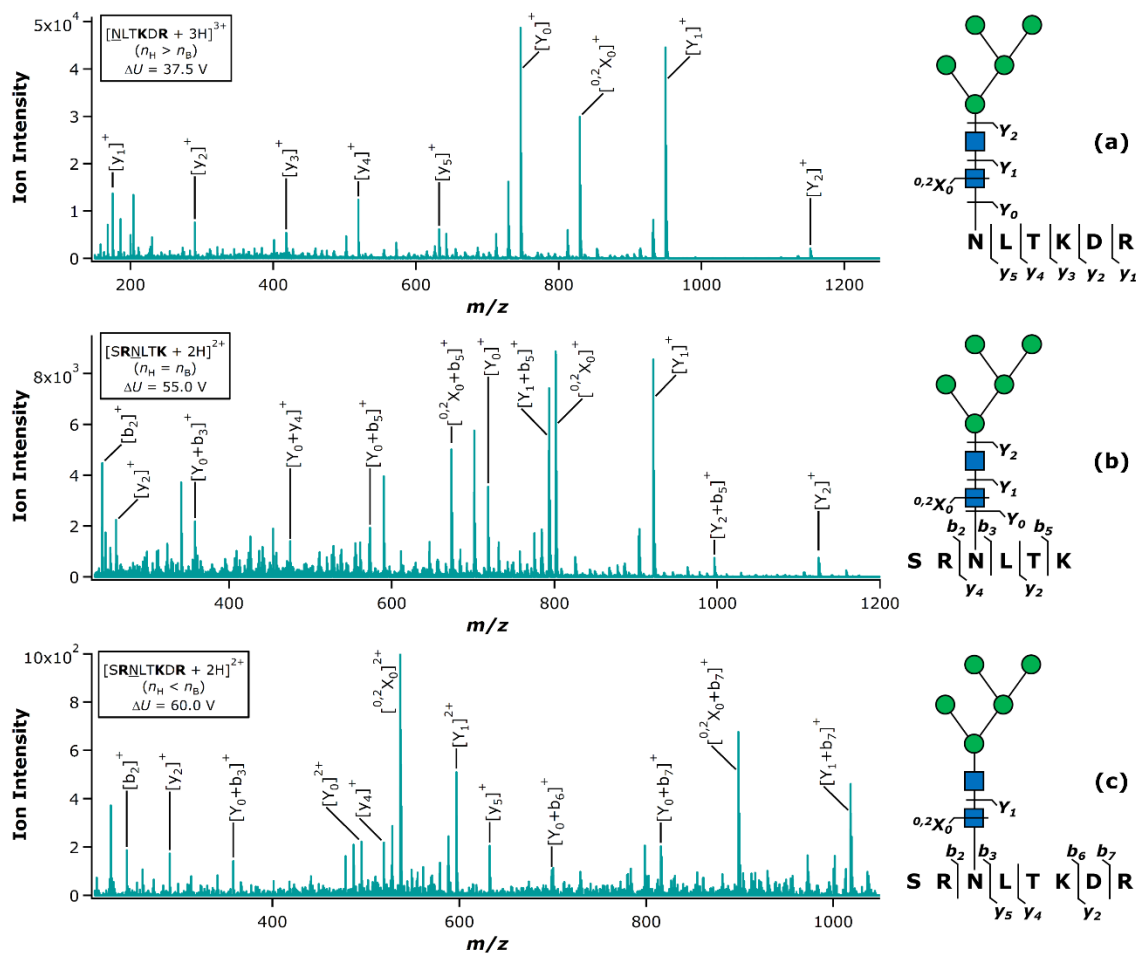


Figure 3.9. CID spectra for the $[\text{NLTKDR} + \text{GlcNAc}_2\text{Man}_5 + 3\text{H}]^{3+}$ (**a**; $n_{\text{H}} > n_{\text{B}}$), $[\text{SRNLTK} + \text{GlcNAc}_2\text{Man}_5 + 2\text{H}]^{2+}$ (**b**; $n_{\text{H}} = n_{\text{B}}$), and $[\text{SRNLTKDR} + \text{GlcNAc}_2\text{Man}_5 + 2\text{H}]^{2+}$ (**c**; $n_{\text{H}} < n_{\text{B}}$). The applied precursor acceleration potentials (ΔU) are indicated, and were chosen to achieve peptide backbone cleavage such that these products constituted approximately 20% of the integrated peak area (cf. **Table 2**). Cleavage maps summarizing the fragmentation of each glycopeptide are provided to the right of each spectrum.

reaching 100.0%, 80.0%, and 71.5%, respectively. In addition to peptide sequence ions, Y_2 , Y_1 , Y_0 , and $^{0,2}X_0$ cleavages were apparent in the spectra. Strikingly, all of the observed peptide sequence ions were singly charged, regardless of the charge state or proton mobility of the initial precursor ions. Moreover, at these collision energies the charge states of all of the Y_i ions were such that these fragments lacked a mobile proton (singly charged in the case of the $[\text{NLTKDR} + \text{GlcNAc}]$ and $[\text{SRNLTK} + \text{GlcNAc}]$ Y_i fragments; doubly charged in the case of the $[\text{SRNLTKDR} + \text{GlcNAc}]$ Y_i fragment). The

tendency of protonated glycopeptide ions is evidently to either lose charge (likely due to production of carbohydrate oxonium ions⁴¹⁻⁴²) to render a Y_I fragment with lower proton mobility than the precursor, or to retain charge in cases where the initial precursor ion had no mobile protons. In all of the cases examined here, this causes the intermediate Y_I fragment (which eventually gives rise to peptide b and y ions) to harbor only nonmobile protons. Thus, protonated glycopeptide ions can behave quite similarly with respect to the vibrational mode normalized collision energies which bring about peptide backbone fragments, even when they greatly differ in the energetics of precursor ion survival and glycan fragment appearance.

Conclusions

This report elaborates on the relation of precursor ion proton mobility to the relative energy requirements for glycan and peptide cleavage in vibrational activation / dissociation of representative N-glycopeptides. Both the 50% precursor ion survival energies and the energies which resulted in optimum production of glycan fragments varied widely among the precursor ions under study, and generally increased with decreasing proton mobility. Conversely, the energies at which peptide backbone fragments were readily accessed exhibited little or no correlation with the proton mobility of the precursor ion. This apparent disconnect is explained by the observation that peptide backbone fragments are products of sequential dissociation, and arise largely from the intermediate Y_I fragment. For all of the cases studied here, the Y_I fragments were produced in charge states that afforded only nonmobile protons, regardless of the charge state or proton mobility of the precursor ion. An important consequence of this finding is

that the degrees of freedom normalized vibrational energy deposition required to render peptide sequence ions was surprisingly similar among the glycopeptide ions studied, even when their other energy-resolved CID characteristics were quite disparate. While further study is needed in order to determine whether these trends are broadly representative of much larger populations of protonated N-glycopeptides, the current results are encouraging in that they suggest the potential that glycan cleavage and peptide cleavage can be deliberately accessed for putative unknowns based on characteristics such as charge state and molecular weight. This, in turn, intimates the possibility of an expanded role for CID in glycoproteomic analysis.

References

1. Morelle, W.; Canis, K.; Chirat, F.; Faid, V.; Michalski, J. C. *Proteomics* **2006**, *6*, 3993-4015.
2. Dalpathado, D. S.; Desaire, H. *Analyst* **2008**, *133*, 731-738.
3. Tissot, B.; North, S. J.; Ceroni, A.; Pang, P.-C.; Panico, M.; Rosati, F.; Capone, A.; Haslam, S. M.; Dell, A.; Morris, H. R. *FEBS Letters* **2009**, *583*, 1728-1735.
4. Levery, S. B.; Steentoft, C.; Halim, A.; Narimatsu, Y.; Clausen, H.; Vakhrushev, S. Y. *Biochimica et Biophysica Acta* **2015**, *1850*, 33-42.
5. North, S. J.; Hitchen, P. G.; Haslam, S. M.; Dell, A. *Current Opinion in Structural Biology* **2009**, *19*, 498-506.
6. Pasing, Y.; Sickmann, A.; Lewandrowski, U. *Biological Chemistry* **2012**, *393*, 249-258.
7. Schiel, J. E. *Analytical and Bioanalytical Chemistry* **2012**, *404*, 1141-1149.
8. Kolli, V.; Schumacher, K. N.; Dodds, E. D. *Bioanalysis* **2015**, *7*, 113-131.
9. Alley, W. R.; Mann, B. F.; Novotny, M. V. *Chemical Reviews* **2013**, *113*, 2668-2732.
10. Desaire, H. *Molecular & Cellular Proteomics* **2013**, *12*, 893-901.
11. Huang, Y.; Gelb, A. S.; Dodds, E. D. *Current Metabolomics* **2013**, *1*, 291-305.
12. Thaysen-Andersen, M.; Packer, N. H. *Biochimica et Biophysica Acta* **2014**, *1844*, 1437-1452.
13. Wührer, M.; Catalina, M. I.; Deelder, A. M.; Hokke, C. H. *Journal of Chromatography B* **2007**, *849*, 115-128.
14. Dodds, E. D. *Mass Spectrometry Reviews* **2012**, *31*, 666-682.

15. An, H. J.; Froehlich, J. W.; Lebrilla, C. B. *Current Opinion in Chemical Biology* **2009**, *13*, 421-426.
16. Nilsson, J.; Halim, A.; Grahn, A.; Larson, G. *Glycoconjugate Journal* **2013**, *30*, 119-136.
17. Zhang, L.; Reilly, J. P. *Journal of Proteome Research* **2008**, *8*, 734-742.
18. Madsen, J. A.; Ko, B. J.; Xu, H.; Iwashkiw, J. A.; Robotham, S. A.; Shaw, J. B.; Feldman, M. F.; Brodbelt, J. S. *Analytical Chemistry* **2013**, *85*, 9253-9261.
19. Adamson, J. T.; Hakansson, K. *Journal of Proteome Research* **2006**, *5*, 493-501.
20. Bindila, L.; Steiner, K.; Schaffer, C.; Messner, P.; Mormann, M.; Peter-Katalinic, J. *Analytical Chemistry* **2007**, *79*, 3271-3279.
21. Seipert, R. R.; Dodds, E. D.; Clowers, B. H.; Beecroft, S. M.; German, J. B.; Lebrilla, C. B. *Analytical Chemistry* **2008**, *80*, 3684-3692.
22. Seipert, R. R.; Dodds, E. D.; Lebrilla, C. B. *Journal of Proteome Research* **2009**, *8*, 493-501.
23. Segu, Z. M.; Mechref, Y. *Rapid Communications in Mass Spectrometry* **2010**, *24*, 1217-1225.
24. Cao, Q.; Zhao, X.; Zhao, Q.; Lv, X.; Ma, C.; Li, X.; Zhao, Y.; Peng, B.; Ying, W.; Qian, X. *Analytical Chemistry* **2014**, *86*, 6804-6811.
25. Kolli, V.; Dodds, E. D. *Analyst* **2014**, *139*, 2144-2153.
26. Aboufazeli, F.; Kolli, V.; Dodds, E. D. *Journal of the American Society for Mass Spectrometry* **2015**, *26*, 587-595.
27. Tajiri, M.; Kadoya, M.; Wada, Y. *Journal of Proteome Research* **2009**, *8*, 688-693.

28. Vekey, K.; Ozohanics, O.; Toth, E.; Jeko, A.; Revesz, A.; Krenyacz, J.; Drahos, L. *International Journal of Mass Spectrometry* **2013**, *345-347*, 71-79.
29. Dongré, A. R.; Jones, J. L.; Somogyi, Á.; Wysocki, V. H. *Journal of American Chemical Society* **1996**, *118*, 8365-8374.
30. Wysocki, V. H.; Tsaprailis, G.; Smith, L. L.; Brechi, L. A. *Journal of Mass Spectrometry* **2000**, *35*, 1399-1406.
31. Varki, A.; Cummings, R. D.; Esko, J. D.; Freeze, H. H.; Stanley, P.; Marth, J. D.; Bertozzi, C. R.; Hart, G. W.; Etzler, M. E. *Proteomics* **2009**, *9*, 5398-5399.
32. Roepstorff, P.; Fohlman, J. *Biomedical Mass Spectrometry* **1984**, *11*, 601.
33. Domon, B.; Costello, C. E. *Glycoconjugate Journal* **1988**, *5*, 397-409.
34. Juhasz, P.; Martin, S. A. *International Journal of Mass Spectrometry and Ion Processes* **1997**, *169/170*, 217-230.
35. An, H. J.; Peavy, T. R.; Hedrick, J. L.; Lebrilla, C. B. *Analytical Chemistry* **2003**, *75*, 5628-5637.
36. Clowers, B. H.; Dodds, E. D.; Seipert, R. R.; Lebrilla, C. B. *Journal of Proteome Research* **2007**, *6*, 4032-4040.
37. Dodds, E. D.; Seipert, R. R.; Clowers, B. H.; German, J. B.; Lebrilla, C. B. *Journal of Proteome Research* **2009**, *8*, 502-512.
38. Memboeuf, A.; Nasioudis, A.; Indelicato, S.; Pollreis, F.; Kuki, A.; Keki, S.; van den Brink, O. F.; Vekey, K.; Drahos, L. *Analytical Chemistry* **2010**, *82*, 2294-2302.
39. Indelicato, S.; Bongiorno, D.; Indelicato, S.; Drahos, L.; Turco Liveri, V.; Turiák, L.; Vékey, K.; Ceraulo, L. *Journal of Mass Spectrometry* **2013**, *48*, 379-383.

40. Kapp, E. A.; Schutz, F.; Reid, G. E.; Eddes, J. S.; Moritz, R. L.; O'Hair, R. A.; Speed, T. P.; Simpson, R. J. *Analytical Chemistry* **2003**, *75*, 6251-6264.
41. Hart-Smith, G.; Raftery, M. J. *Journal of the American Society for Mass Spectrometry* **2012**, *23*, 124-140.
42. Froehlich, J. W.; Dodds, E. D.; Wilhelm, M.; Serang, O.; Steen, J. A.; Lee, R. S. *Molecular & Cellular Proteomics* **2013**, *12*, 1017-1025.

Appendix A

Brief Summary of This Work

The work presented in this thesis emphasizes that the application of energy-resolved collision-induced dissociation can yield significant coverage of both the monosaccharide connectivity and the amino acid sequence of protonated N-linked glycopeptide ions. As a general principle, increasing collision energies lead to multiple, consecutive generations of product ions that appear in a particular order: $Y_{n>1}$ glycan cleavages (primary fragment ions), Y_1 glycan cleavage (secondary fragment ions), and b , y peptide cleavages (tertiary fragment ions). This qualitative behavior applies to all protonated N-glycopeptides studied here, regardless of charge state, glycan type, or peptide composition. However, the quantitative relationships between collision energies and fragment ion types did vary considerably among different analyte ions. These quantitative differences were explained in part by precursor ion proton mobility. Proton mobility of the precursor ion was found to correlate negatively with the collision energies required to deplete the precursor ion, and to produce primary fragmentation products ($Y_{n>1}$ glycan fragments). By contrast, the production of peptide b and y ions was found to have no relation to precursor ion proton mobility. This is consistent with the observation that the peptide b and y cleavages are tertiary fragment ions, arising from the secondary Y_1 fragment ions. The apparent disconnect between the precursor ion proton mobility and the collision energies needed to produce peptide fragmentation is also in accord with the observation that Y_1 fragment ions generally have lower proton mobilities than their respective precursor ions (largely due to loss of charge to carbohydrate oxonium ions). Overall, these results suggest the possibility that precursor ion characteristics, including proton mobility, can be predictive of the collision energies needed to intentionally access glycan or peptide cleavage products.